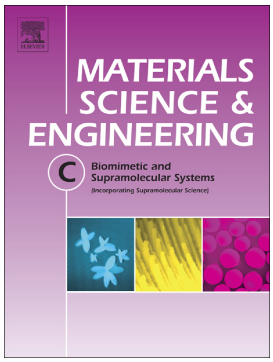

Controlled degradability of PCL-ZnO nanofibrous scaffolds for bone tissue engineering and their antibacterial activity

Betiana Felice, María Alejandra Sánchez, María Cecilia Socci, Luciano David Sappia, María Inés Gómez, María Karina Cruz, Carmelo José Felice, Mercè Martí, María Isabel Pividori, Gabriela Simonelli, Andrea Paola Rodríguez

PII:	S0928-4931(18)30524-1
DOI:	doi:10.1016/j.msec.2018.08.009
Reference:	MSC 8803
To appear in:	*Materials Science & Engineering C*
Received date:	3 March 2018
Accepted date:	5 August 2018

Please cite this article as: Betiana Felice, María Alejandra Sánchez, María Cecilia Socci, Luciano David Sappia, María Inés Gómez, María Karina Cruz, Carmelo José Felice, Mercè Martí, María Isabel Pividori, Gabriela Simonelli, Andrea Paola Rodríguez , Controlled degradability of PCL-ZnO nanofibrous scaffolds for bone tissue engineering and their antibacterial activity. Msc (2018), doi:10.1016/j.msec.2018.08.009

Controlled degradability of PCL-ZnO nanofibrous scaffolds for bone tissue engineering and their antibacterial activity

Betiana Felice[1,2], María Alejandra Sánchez[1,2], María Cecilia Socci[1,2], Luciano David Sappia[1,2], María Inés Gómez[3], María Karina Cruz[3], Carmelo José Felice[1,2], Mercè Martí[4,5], María Isabel Pividori[4], Gabriela Simonelli[6], Andrea Paola Rodríguez[1,2]

[1] Laboratorio de Medios e Interfases, Departamento de Bioingeniería, Facultad de Ciencias Exactas y Tecnología, Universidad Nacional de Tucumán, Av. Independencia 1800, CP4000, Tucumán, Argentina*

[2] Instituto Superior de Investigaciones Biológicas, Consejo Nacional de Investigaciones Científicas y Técnicas, Chacabuco 461, CP4000, Tucumán, Argentina

[3] Instituto de Química Inorgánica, Facultad de Bioquímica, Química y Farmacia, Universidad Nacional de Tucumán, Ayacucho 471, CP4000, Tucumán, Argentina

[4] Grup de Sensors i Biosensors, Departament de Química, Universitat Autònoma de Barcelona, 08193 Bellaterra, Spain

[5] Immunology Unit, Institut de Biotecnologia i de Biomedicina (IBB), Universitat Autònoma de Barcelona, 08193 Cerdanyola del Vallès (Bellaterra), Spain

[5] Departament de Biologia Cel·lular, Fisiologia i Immunologia (BCFI), Universitat Autònoma de Barcelona, 08193 Cerdanyola del Vallès (Bellaterra), Spain

[6] Laboratorio de Física del Sólido, INFINOA (CONICET-UNT), Facultad de Ciencias Exactas y Tecnología, Universidad Nacional de Tucumán, Av. Independencia 1800, CP4000, Tucumán, Argentina

Corresponding author: Dr. Andrea P. Rodríguez

E-mail: aprodriguez@herrera.unt.edu.ar

Telephone: +54 381 4364120

ABSTRACT

Up to date, tissue regeneration of large bone defects is a clinical challenge under exhaustive study. Nowadays, the most common clinical solutions concerning bone regeneration involve systems based on human or bovine tissues, which suffer from drawbacks like antigenicity, complex processing, low osteoinductivity, rapid resorption and minimal acceleration of tissue regeneration. This work thus addresses the development of nanofibrous synthetic scaffolds of polycaprolactone (PCL) - a long-term degradation polyester - compounded with hydroxyapatite (HA) and variable concentrations of ZnO as alternative solutions for accelerated bone tissue regeneration in applications requiring mid- and long-term resorption. *In vitro* cell response of human fetal osteoblasts as well as antibacterial activity against *Staphylococcus aureus* of PCL:HA:ZnO and PCL:ZnO scaffolds were here evaluated. Furthermore, the effect of ZnO nanostructures at different concentrations on *in vitro* degradation of PCL electrospun scaffolds was analyzed. The results proved that higher concentrations ZnO may induce early mineralization, as indicated by high alkaline phosphatase activity levels, cell proliferation assays and positive Alizarin-Red-S-stained calcium deposits. Moreover, all PCL:ZnO scaffolds particularly showed antibacterial activity against *S. aureus* which may be attributed to release of Zn^{2+} ions. Additionally, results here obtained showed a variable PCL degradation rate as a function of ZnO concentration. Therefore, this work suggests that our PCL:ZnO scaffolds may be promising and competitive short-, mid- and long-term resorption systems against current clinical solutions for bone tissue regeneration.

Keywords: Bone Tissue Engineering; ZnO; Polycaprolactone; Degradation rate; Mineralization; Antibacterial

1. INTRODUCTION

Large bone defects are still a clinical challenge. Up to date, defects caused by e.g. trauma, infection or tumor removal are usually treated either with autografts, allografts or xenografts [1–3]. However, donor-site morbidity related to autografts, high-costs of allografts, antigenicity and poor mechanical properties of natural grafts in addition to their complex manufacturing suggest that synthetic bone grafts provide a better solution [1–3]. Then, electrospun synthetic scaffolds of polycaprolactone (PCL) compounded with hydroxyapatite (HA) and zinc oxide (ZnO) emerge as promising alternatives against natural grafts.

PCL is a semicrystalline polyester extensively studied, with an outstanding biocompatibility *in vitro* and *in vivo* [4,5]. Such features, in addition to the degradability of its ester bonds upon hydrolysis, turns PCL into a commonly used polymer in several devices approved by the U.S. Food and Drug Administration [6–8]. However, as this polymer lacks of specific cues for bone regeneration, further modifications are mandatory in order to optimize bone growth on PCL[9] . Given the flexibility of its chains at room temperature, its ability to be combined with multiple materials and its solubility in a large amount of organic solvents, PCL can be prepared for bone regeneration by means of combination with osteoactive materials followed by processing via electrospinning [10].

Nanofibrous scaffolds obtained through electrospinning mimic the extracellular matrix of immature bone, which is characterized by randomly organized fibrous collagen structures with diameters ranging from 10 to 300 nm [11–13]. Considering that osteoblasts are adherent cells, it was reported that the topography of electrospun scaffolds promotes osteoblasts adhesion, migration and proliferation [11]. Such modification provides the physical cues for bone regeneration, whereas chemical signaling related to bone growth primarily results from

combination of PCL with osteoactive materials. HA is a ceramic with low degradability rate and high osteoconductivity caused by its resemblance with mineral components of natural bone matrix [14]. Many authors have previously reported the combination of PCL, polylactic acid (PLA) and polylactic-co-glycolic acid (PLGA) with HA as a coating or filler in bone tissue engineering (BTE) applications [15–17]. Likewise, ZnO promotes bone growth. However, its action mechanism is based on induction and acceleration of bone tissue regeneration in addition to active prevention of bacterial infections which may hinder tissue healing.

ZnO is an inorganic material able to exert osteoinductive and osteoconductive effects. In particular, ZnO osteoinductivity was observed by Yusa *et al* on mesenchymal cells cultured on surfaces releasing Zn^{2+} ions [18]. These authors suggested that Zn^{2+} ions induce osteoblast differentiation by means of a significant increase of gene expression of col I (collagen I, most common protein of bone extracellular matrix), BMP-2 (bone morphogenetic protein, which induces mineralization of the extracellular matrix), alkaline phosphatase (biological marker of mineralization beginning), Runx2 (transcription factor that induces differentiation of mesenchymal cells into osteoblasts) and VEGF-A (angiogenic factor) [18].

Furthermore, ZnO is widely recognized as an effective non-specific antibacterial agent against a broad spectrum of microorganisms [19]. Bacterial infections are among the commonest causes of bone graft failure [20–22]. Nowadays, mild infections are usually treated with antibiotics whereas advanced infections involve not only antibiotics but also graft removal, cleaning of the damaged area and implanting a new graft, thus exposing the patient to several surgeries which even increase re-infection risk of the treated tissue [23]. Moreover, frequent use of antibiotics implies higher risk for developing drug-resistant microorganisms like methicillin-resistant *Staphylococcus aureus* [24]. Consequently, scaffolds for BTE

manufactured with materials functionalized with ZnO are promising alternatives to current antibacterial solutions.

An ideal polymeric scaffold for BTE should not only be degradable but also its degradation time should match tissue regeneration time in order to guarantee the structural integrity until formation of new tissue. The latter physiological process normally requires between 2 and 6 months (or even more) primarily depending on bone defect size [25]. Thus, time matching represents up to date a challenge concerning the design of degradable PCL scaffolds for BTE. PCL is slowly degraded under physiological conditions through deesterification by hydrolysis followed by phagocytosis when the molecular weight is below 3000 Da [26]. It has been reported that the total degradation of PCL homopolymer, depending on initial molecular weight, takes between 1 and 4 years, period of time that hinders the use of PCL at short- and mid-term applications concerning BTE [27]. Up to date, PCL degradation time was decreased either by copolymerization or mixture with other lactones, polylactic acid and polyglycolic acid or by compounding of PCL with particles like hydroxyapatite, silicates and β-TCP (Tricalcium Phosphate) [27–30]. Although the latter technique have been already reported, the action mechanism of compounded particles on PCL degradation rate remains uncertain given that it is a function of multiple factors like chemical nature, particle size and polymer-microenvironment interactions [31,32].

Hence, this work addresses the synthesis via electrospinning of scaffolds of PCL compounded with HA and variable concentrations of ZnO for bone tissue engineering. In order to determine their suitability for bone tissue regeneration, *in vitro* response of human fetal osteoblasts cultured on different electrospun scaffolds is here evaluated. In addition, the antibacterial response of the scaffolds against *Staphylococcus aureus* is systematically studied. Furthermore, here we evaluate the degradation of PCL electrospun scaffolds for BTE

in terms of nanostructured ZnO concentration as an alternative mechanism for regulation of PCL degradation rate. Degradation effects are analyzed by means of scanning electron microscopy, dynamic thermal analysis, mechanical properties, wettability and FTIR spectroscopy.

2. MATERIALS AND METHODS

2.1 Materials

For scaffold fabrication, PCL (80000 Da) and ZnO nanopowder were purchased from Sigma Aldrich (Argentina). Bovine HA was kindly provided by Idear SRL (Argentina). Chloroform and dimethylformamide (DMF) were obtained from Sintorgan (Argentina). For *in vitro* evaluation of our scaffolds, human fetal osteoblast cell line (HFOb 1.19) was purchased from the Eucellbank (Barcelona, Spain). For cell culture, Dulbecco's Modified Eagle's Medium (DMEM), F-12, Fetal Bovine Serum (FBS) and L-Glutamine 200 mM were acquired from Lonza (Spain). Geneticin and Penicillin-Streptomycin 100x were provided by Sigma Aldrich (Spain). Antibacterial activity was evaluated against the gram-positive strain *Staphylococcus aureus* subsp. *Aureus* (ATCC® 25293™), kindly provided by Dr. Miguel Fernández de Ulivarri. Yeast extract, Peptone from Casein (pancreatic digest) and agar-agar were purchased from Neogen (Argentina). Glycerin and salts were acquired from Biopack (Argentina). All assays were performed under biosafety conditions level 2.

2.2 Electrospinning of scaffolds

For scaffold fabrication, a suspension of ZnO nanopowder was prepared in chloroform at a concentration of 8 %w/v. In order to obtain at final scaffolds a variable concentration of ZnO, different volumes of the suspension were mixed with DMF, keeping in all cases the ratio chloroform:DMF at 4:1 respectively. The mixtures were then homogenized and further blended with PCL pellets at 8 %w/v, followed by an overnight stirring.

The solutions thus obtained were separately loaded in 5 ml syringes and a high voltage of 8 kV (High Voltage System, ALMA, Argentina) was applied. A positively charged jet was formed from the 22G syringe needle and nanofibers were sprayed onto a grounded aluminum film kept 15 cm away from the tip of the needle. Mats were dried for a week under room conditions. Table 1 summarizes the composition of the samples which were evaluated in this work.

Table 1. Samples. Scaffolds prepared for further assessment of *in vitro* response and antibacterial activity. Polymer concentration is expressed in terms of %w/v respect to solution volume, whereas HA and ZnO concentrations are expressed in terms of wt% respect to polymer weight.

	Sample	Description
	PCL	8 % w/V PCL
With HA	**PCL:HA**	8 % w/V PCL 15 w% HA
With ZnO	**PCL:ZnO 1%**	8 % w/V PCL 1 w% ZnO
	PCL:ZnO 3%	8 % w/V PCL 3 w% ZnO
	PCL:ZnO 6%	8 % w/V PCL 6 w% ZnO
With HA and ZnO	**PCL:HA:ZnO 1%**	8 % w/V PCL 15 w% HA 1 w% ZnO
	PCL:HA:ZnO 3%	8 % w/V PCL 15 w% HA 3 w% ZnO
	PCL:HA:ZnO 6%	8 % w/V PCL 15 w% HA 6 w% ZnO

2.3 Morphology study

Morphology analysis as well as distribution of ZnO nanopowder within the fibers was performed through scanning electron microscopy (SEM). Samples were previously sputter coated with gold (JEOL JFC-1200, Japan) and further visualized with a Zeiss Supra 55VP (Carl Zeiss GmbH, Germany). Images were obtained using backscattered electrons at an accelerating voltage of 20 kV in order to analyze particle distribution within the fibers. SEM images were processed using the software Image J (National Institute of Health, United States).

2.4 HFOb culture

HFOb 1.19 (henceforth named HFOb) cells were cultured in 75 cm^2 flasks using DMEM:F-12 (1:1) containing 10% of FBS, 1% of Penicillin-Streptomycin, 0.9% of L-Glutamine and 0.6% of Geneticin. Cells were maintained in a humidified CO_2 incubator, fed with fresh media after every 3 days and trypsinized using trypsin-EDTA for cell seeding experiments. HFOb of passages 4 to 6 were used during this study.

For cell response evaluation, the scaffolds (Ø=13mm) previously described in table 1 were sterilized by immersion in ethanol 70% for 60 minutes and further rinsed with sterile PBS. Subsequently, such samples were immersed overnight in culture medium to promote cell adhesion. The scaffolds were then placed in 24-multiwell plates and irradiated with UV-light for 15 minutes. Finally, HFOb were seeded at a density of $20x10^3$ cells/cm^2 on each scaffold and on tissue culture polystyrene as control.

2.5 Cell proliferation study

Cell proliferation on different electrospun scaffolds was monitored after 3, 7 and 14 days by MTT assay (3-(4,5-methylthiazol-2-yl)-2,5-diphenyltetrazolium bromide), employing the Vybrant® MTT kit (Life Technologies, United States). Metabolically active cells react with

the tetrazolium salt in MTT reagent to produce soluble formazan dye that can be measured at 570 nm. After desired periods, the cell-scaffold constructs were rinsed with PBS and incubated with 0.05% MTT reagent for 4 hours at 37°C, according to provider instructions. Formazan salts produced were then solubilized in SDS at 37°C for 18 hours. Finally, aliquots were pipetted into 96-multiwell plates and the samples were read using a microplate reader model TECAN Sunrise (Tecan Group Ltd, Switzerland).

2.6 Determination of alkaline phosphatase activity

Alkaline phosphatase (ALP) activity was spectrophotometrically measured by *p*-nitrophenyl phosphate (*p*NPP) method. ALP expression is an indicator of bone-forming ability of HFOb seeded on different scaffolds [33]. ALP catalyzes *p*NPP hydrolysis to produce inorganic phosphates and *p*-nitrophenol, which is detected at 405 nm. Therefore, cells were cultured for 3, 7 and 14 days and assessed for their ALP activity. Cell-scaffold constructs were washed with PBS, followed by addition of 10 mM *p*NPP (Sigma Aldrich, Spain) dissolved in buffer DEA and then incubated for 30 minutes at room temperature and under constant stirring. The reaction was stopped using 2N NaOH and aliquots were pippeted into 96-multiwell plates in order to measure absorbance at 405 nm using a microplate reader. Results were finally normalized with respect to the number of cells per well.

2.7 Mineralization assay

The dye Alizarin Red S (ARS) selectively binds to calcium salts and is widely used for calcium mineral histochemistry. During this study, detection and quantification of calcium deposits were then performed through ARS staining. Cell-scaffold constructs cultured for 14 days were washed twice with PBS and later fixed with ethanol 70% for 60 minutes at 4°C. Subsequently, they were washed with distilled water, incubated with 40 mM ARS for 30 minutes at room temperature and repeatedly rinsed with distilled water in order to discard

ARS excess. The constructs were desorbed by incubating the samples in 10% acetic acid for 30 minutes at room temperature under mild stirring. Supernatants and samples were then vortexed for 30 seconds and incubated at 85°C for 10 minutes. Supernatants were cooled down and centrifuged at 20000 g for 15 minutes. Finally, aliquots were pipetted into 96-multiwell plates and absorbance was measured at 405 nm using a microplate reader. The background absorbance of the scaffolds caused by HA-content was determined by processing scaffolds without cells. The final absorbance was then obtained by subtracting the background adsorption values.

2.8 Antibacterial activity assessment

For assessment of the antibacterial activity, a group of samples was further subjected to *in vitro* degradation by immersion in PBS at 37°C for 0 and 30 days. Samples were then rinsed with distilled water, dried at room temperature and subjected to microbiological evaluation. Samples degraded for 0 days were also microbiologically evaluated as a control. In all cases, each assay was repeated three times (n=3) by processing three replicates each assay (i=3).

For evaluation of antibacterial response against *Staphylococcus aureus*, samples were cut (10x10 mm^2), sterilized by immersion in ethanol 70% for 60 minutes, washed three times with sterile PBS and finally irradiated with UV-light for 15 minutes.

In vitro antibacterial activity of our scaffolds against *S. aureus* was evaluated through a modified dilution method based on the standard *CLSI M07-A9: Methods for dilution antimicrobial susceptibility tests for bacteria that grow aerobically* (Cockeril et al. 2012). Firstly, *S. aureus* was cultured in Luria-Bertani-Miller (LBM) broth (10 g/l Casein Peptone, 5 g/l Yeast extract and 10 g/l NaCl), incubated at 37°C for 16-18 hours and stored in LBM broth with 10% Glycerol. Before each assay, 5 ml of LBM broth were inoculated with $1x10^8$ CFU/ml and incubated at 37°C until they achieved a turbidity equivalent to a 0.5 McFarland

turbidity standard. Subsequently, the inocule was diluted in PBS to obtain $5x10^5$ CFU/ml. Sterile samples were then immersed in 1 ml of inocule previously prepared and incubated for 18 hours at 35±2°C. The survival colony forming units (CFU/ml) were determined by the plate count agar method in LBM. Final results were normalized with respect to the sample area and inoculation volume in order to express them as log CFU/cm^2.

2.9 Degradation assays

The scaffolds were degraded and further assessed according to ISO 10993-13: *Identification and quantification of degradation products from polymeric medical devices* and further [34]. Samples were cut as rectangles (4 cm x 1 cm) and subsequently immersed in 20 mL of phosphate buffer saline (PBS, pH 7.4) and incubated at 37 °C for 5 and 15 days. Degradation medium was replaced by fresh PBS every 3 days. Finally, samples were rinsed with distilled water and dried at room temperature. A group of samples was further freezed-dried in order to quantify material wettability by means of contact angle.

2.10 Mechanical properties

Mechanical properties of samples after 0,5 and 15 days of degradation were determined through mechanical stress tests performed by a dual-column universal testing system model Instron-3369 equipped with a 5 kN load cell. Samples were cut as rectangles (45 mm x 10 mm), clamped with an initial separation distance of 25 mm and the stress rate was set at 25 mm/min. At least 5 specimens per samples were subjected to mechanical stress and their corresponding signals were analyzed using OriginPro software (MicroCal Software, Inc, United States). Young modulus, ultimate tensile strength and strain at fracture were determined.

2.11 Wettability: Measurement of contact angle

Wettability of samples was determined in terms of water contact angle measured according to the sessile drop method under room conditions by using a DSLR camera model Nikon D750 equipped with a lens with a focal distance of 28 mm and 8 MP resolution. PCL, PCL:HA, PCL:ZnO and PCL:HA:ZnO scaffolds with different ZnO contents and subjected to different incubation times in PBS (0, 5 and 15 days) were placed on a flat surface between the light source and the camera. 6 μL droplets of distilled water -according to ISO 55660-2- were pipetted on sample surface and pictures were recorded after 10 seconds [35]. Images were then pre-processed using Image J (National Institute of Health, United States) and subsequently analyzed by SCA 20 software (Dataphysics Instruments, Germany). At least three specimens per sample were evaluated.

2.12 Differential Thermal Analysis

Glass transition temperature of PCL is -60°C and its melting point is between 59 and 64°C, depending on crystallinity percentage [10]. Additives like fillers significantly affect material crystallization. Then, thermal behavior was evaluated through Differential Thermal Analysis (DTA). A DTA device model DTA-50 (Shimadzu, Japan) was used. Specimens weighing 5 mg were heated up from room temperature to 150 °C at 20 °C/min and under nitrogen atmosphere at a constant flow of 20 mL/min. Crystallization temperature (Tc) as well as melting temperature (Tm) were obtained from exothermic and endothermic peaks respectively.

2.13 Infrared spectroscopy

In order to detect changes at functional groups of our scaffolds after degradation, Fourier Transform Infrared (FTIR) spectroscopy was accomplished. A FTIR device model Nicolet 5700 (Thermo Nicolet, United States) equipped with DTGS detector and air purge system (Parker-Balston, United States) was used. Samples were cut and hold on an air window to

measure infrared transmission between 400 and 4000 cm^{-1}. Spectra were obtained with 2 cm^{-1} resolution and after 32 iterations.

2.14 Statistical analysis

Results are shown as mean±standard deviation. Variance analysis in all cases was done through Levene test with a significance level of 0.05. For mean values comparison (equal variance) of more than three data groups, One-Way ANOVA in combination with *post hoc* Tukey HSD test was applied. Direct comparison of two populations was performed through Student's t-test for unpaired samples. For non-equal variances, Welch test for direct comparison of means was applied. Significance levels are reported at each assay.

3. RESULTS

3.1 Morphology study

Nanofibrous topography of scaffolds plays a key role during initial regulation of cell adhesion and proliferation. Scaffolds morphology and particle distribution within fibers were studied through SEM, as it is shown in Figure 1. Cell response was evaluated against PCL and PCL:ZnO scaffolds containing 1, 3 and 6 wt% of ZnO with resulting fiber diameters of 0.58±0.28 μm, 0.56±0.17 μm, 0.43±0.16 μm and 0.57±0.27 μm respectively. Scaffolds of PCL:HA and PCL:HA:ZnO 1, 3 and 6 % both compounded with 15 wt% HA were also assessed. In this case, fibers diameters were 0.53±0.21 μm, 0.57±0.23 μm, 0.77±0.22 μm and 0.68±0.20 μm respectively. Higher contents of HA would lead to fragile structures and consequently, cracks. It must be noted that HA particles within the fibers are significantly larger than ZnO nanostructures and agglomerates. Furthermore, it can be seen that higher concentrations of ZnO nanopowder induce both higher amounts of ZnO agglomerates as well as larger ZnO agglomerates. Such effect is clearly visible at PCL:ZnO 6% scaffolds. Then, the SEM micrographs obtained with backscattered electrons suggest that ZnO dispersion

along the fibers strongly depends on ZnO nanopowder concentration. However, it is worth mentioning that fiber features are kept uniform showing only a significant increase of diameter for PCL:HA:ZnO 3 and 6% samples ($p \leq 0.05$).

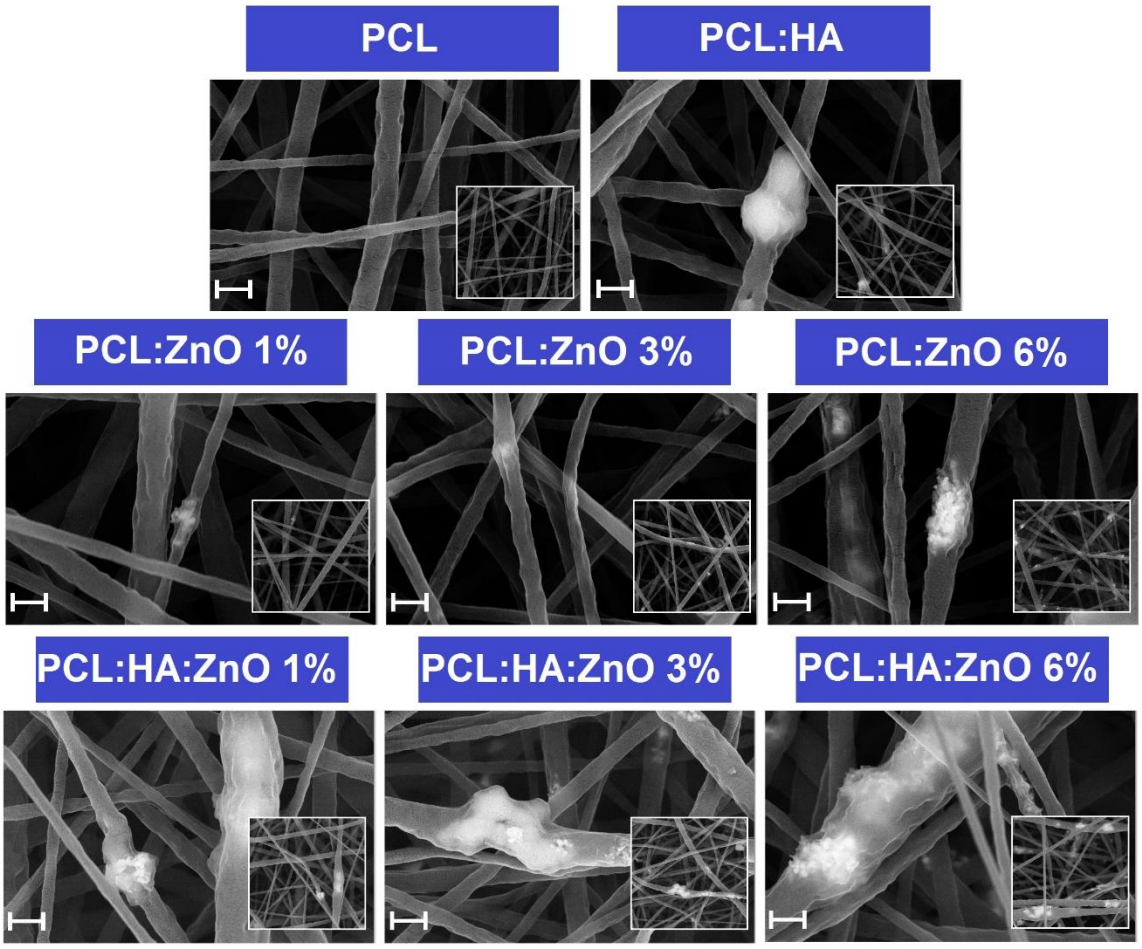

Figure 1 **SEM with backscattered electrons.** Micrographs of scaffolds with different ZnO contents. Magnification bars equal to 1 μm.

3.2 Cell proliferation study

HFOb proliferation was evaluated after 3, 7 and 14 days of culture on PCL, PCL:HA, PCL:ZnO and PCL:HA:ZnO nanofibrous scaffolds. As shown in Figure 2, on PCL and

PCL:HA:ZnO 1%, cell proliferation exponentially growths over time whereas on remaining samples, proliferation is constant from day 3 (PCL:ZnO 6%, PCL:HA:ZnO 3/6%) or from day 7 (PCL:HA, PCL:ZnO 1/3%) ($p \leq 0.05$). Additionally, it should be highlighted that the proliferation at day 14 on PCL samples is between 2 a 10 times larger than cell proliferation on PCL:HA, PCL:ZnO and PCL:HA:ZnO. Moreover, it is observed that higher concentrations of ZnO might induce lower cell proliferation. Hence, it is inferred that ZnO nanopowder addition might induce a decrease of cell proliferation. In addition, such effect seems to oppose PCL effect on HFOb proliferation.

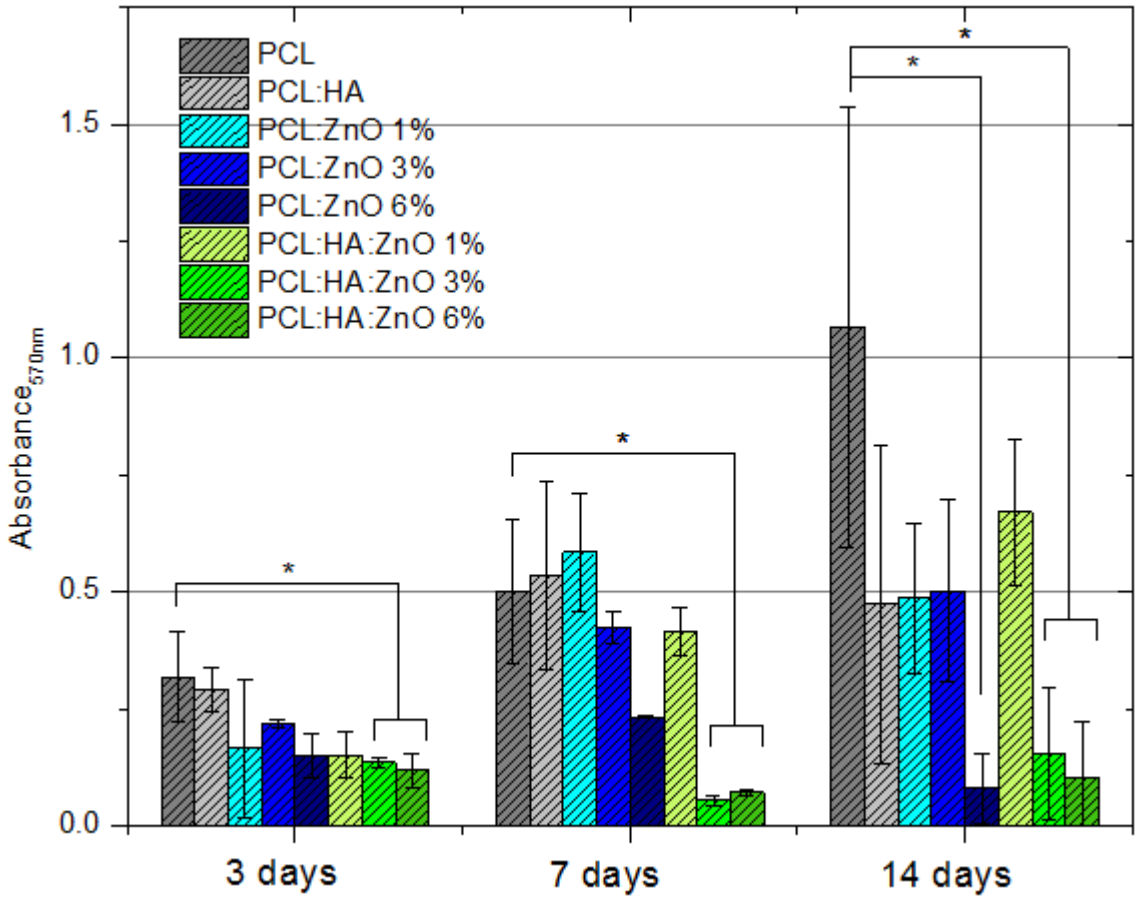

Figure 2 **HFOb proliferation on scaffolds.** HFOb proliferation on PCL, PCL:HA, PCL:ZnO 1, 3 and 6% and PCL:HA:ZnO 1, 3 and 6% determined by MTT assay. *Statistical significance against cell proliferation on PCL for the same period of culture ($p \leq 0.05$) (n=3, i=3).

3.3 Determination of alkaline phosphatase activity

ALP is an enzyme that catalyzes the hydrolysis of extracellular phosphate esters towards inorganic phosphate, necessary for further synthesis and transport of vesicles to the bone extracellular microenvironment [36]. An increase of ALP activity correlated with a constant cell proliferation is a biomarker of mineralization initiation [36–38]. ALP activity of HFOb cultured for 3, 7 and 14 days on PCL, PCL:HA, PCL:ZnO and PCL:HA:ZnO is shown in Figure 3.

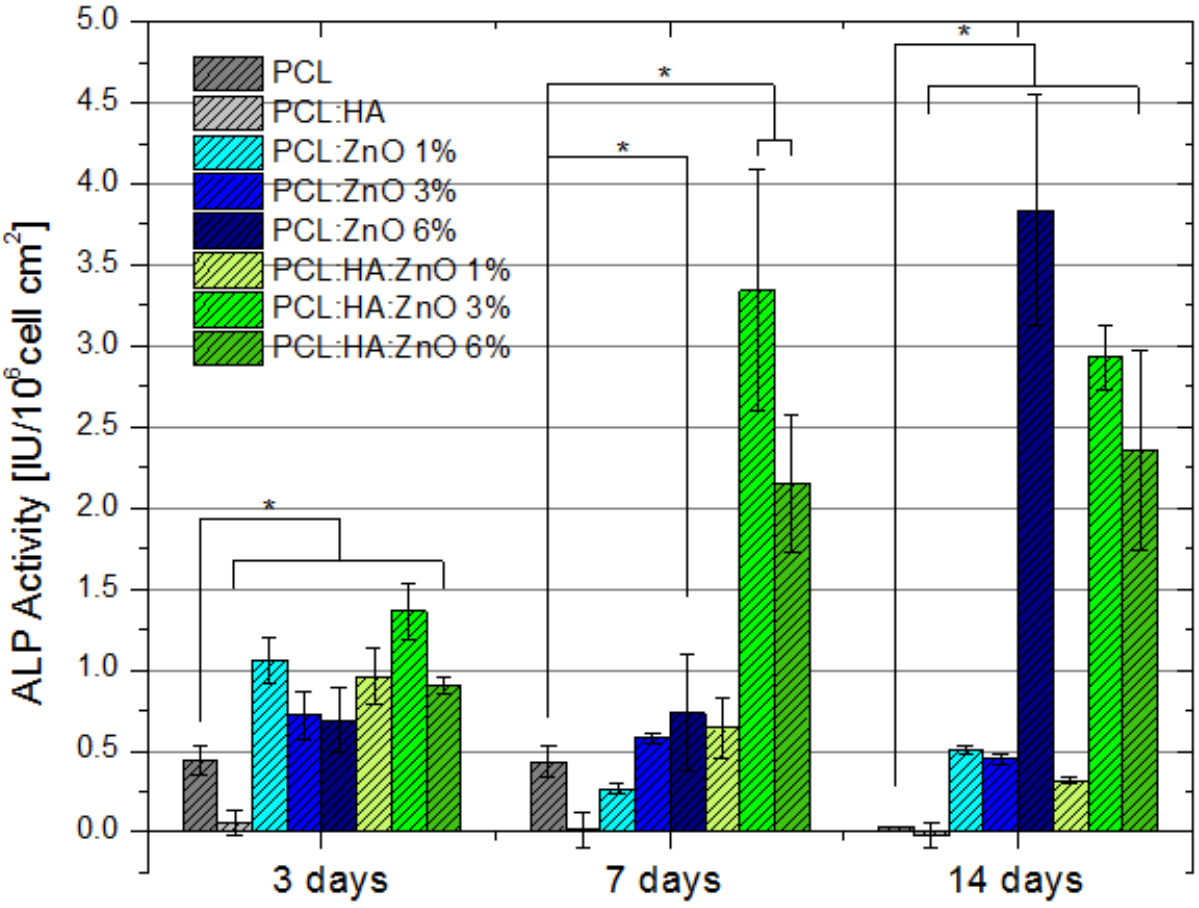

Figure 3 **Activity of alkaline phosphatase.** ALP activity of HFOb cultured on PCL, PCL:HA, PCL:ZnO

1, 3 and 6% and PCL:HA:ZnO 1, 3 and 6% colorimetrically determined. *Statistical significance against ALP activity on PCL for the same period of culture ($p \leq 0.05$) (n=3, i=3).

As observed, ALP activity exponentially increases over time from day 3 on PCL:ZnO 6%, PCL:HA:ZnO 3% and PCL:HA:ZnO 6% samples, reaching a maximum at day 14. On the contrary, ALP activity on remaining samples is either constant or decreases over time, except for the activity registered on PCL:ZnO 1%, which increases from day 7 ($p \leq 0.05$). At day 14 of culture, ALP activity on PCL:ZnO 6% and PCL:HA:ZnO 3 and 6 % is 141, 107 y 86 times higher than the activity measured on PCL samples, respectively. It is worth mentioning that on samples with HA combined with ZnO, ALP activity does not increase in comparison to samples with only ZnO.

Alkaline phosphatase activity results suggest an early initiation of mineralization on PCL:ZnO 6% and PCL:HA:ZnO 3 and 6% as well as a lack of or late mineralization on the other samples under study. Such results will be further discussed in following sections.

3.4 Mineralization assay

ARS staining was here used to quantify calcium deposits formed by HFOb cultured on scaffolds with different contents of ZnO. Figure 4 shows the results at day 14 of culture.

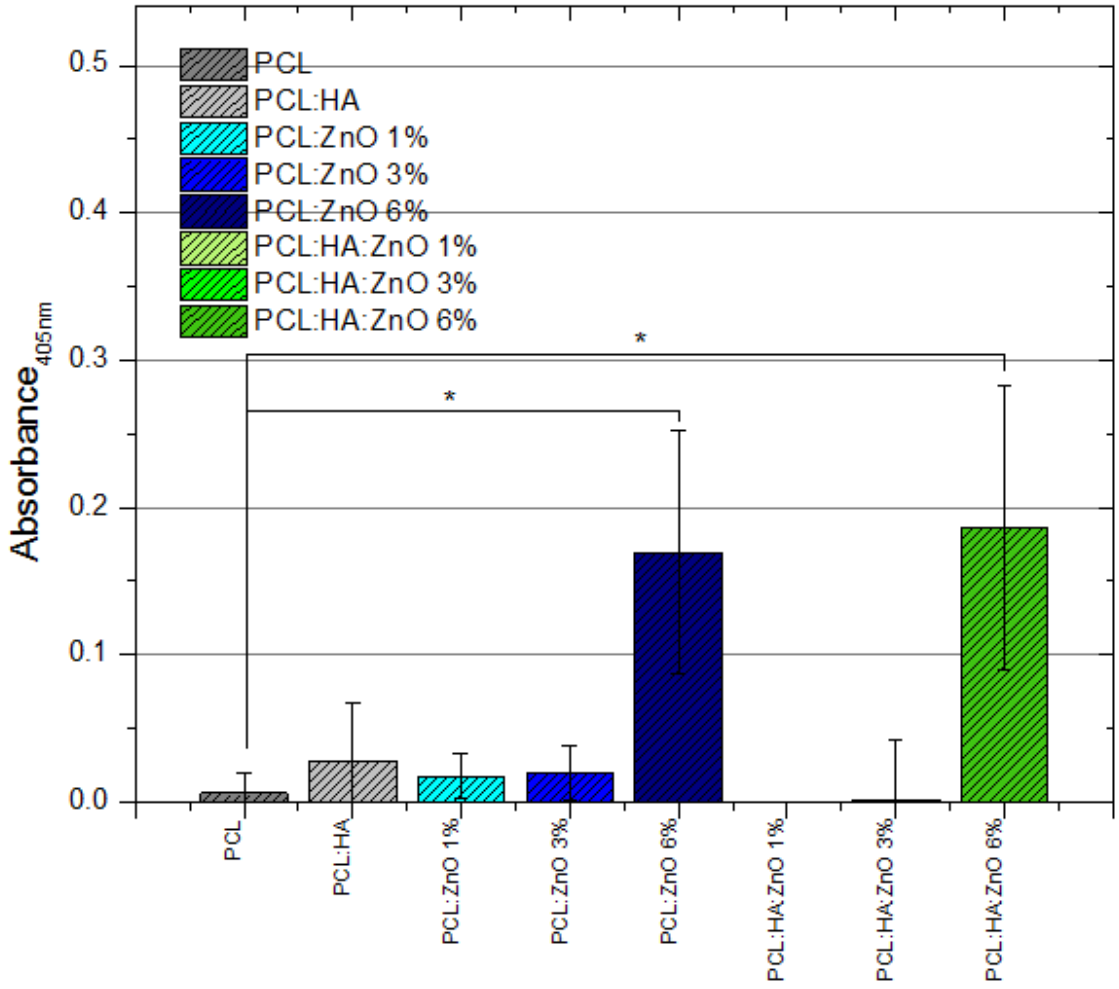

Figure 4 **Mineralization.** Quantitative ARS staining of calcium deposits on PCL, PCL:HA, PCL:ZnO 1, 3 and 6% and PCL:HA:ZnO 1, 3 and 6% at day 14 of culture.*Statistical significance against mineralization on PCL ($p \leq 0.05$) (n=2, i=3).

As it can be observed, the absorbance values of eluents collected from PCL:ZnO 6% and PCL:HA:ZnO 6% are significantly higher than those related to remaining samples. At day 14 of culture, mineralization on PCL:ZnO 6% and PCL:HA:ZnO 6% was found to be 27 y 30 times higher in comparison to mineralization on PCL, respectively. A considerable lower mineralization is observed on the other tested samples, which supports the hypothesis claimed at the previous section regarding late mineralization on PCL, PCL:HA, PCL:ZnO 1/3% and PCL:HA:ZnO 1%.

3.5 Antibacterial activity assessment

Antibacterial activity of the scaffolds towards *S. aureus* was evaluated following a modified dilution method based on a CLSI standard. Figure 5 shows the survival CFU after 18 hours of incubation at 35°C on samples with 0 and 30 days of degradation and as a function of ZnO concentration.

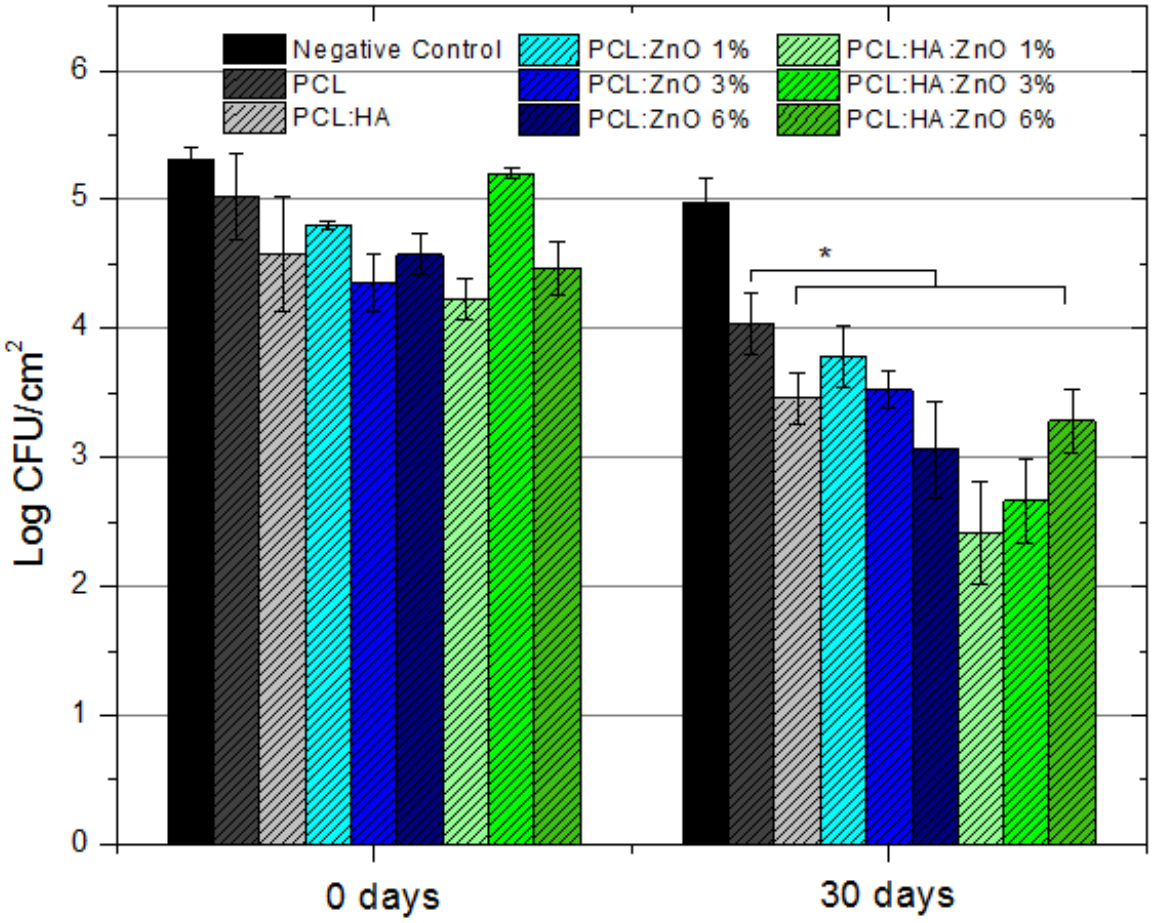

Figure 5 **Antibacterial activity of scaffolds.** Log CFU/cm^2 as a function of ZnO content for samples subjected to 0 and 30 days of *in vitro* degradation. * Statistical significance against PCL for the same period ($p \leq 0.05$) (n=3, i=3).

As it can be observed in Figure 5, at day 0 of degradation, samples with ZnO induce a significant decrease of initial bacterial load in comparison to the negative control ($p \leq 0.05$). Particularly, higher concentrations of ZnO tend to induce antibacterial activity with higher intensity ($p \leq 0.5$). Also, it is worth mentioning that samples with HA and ZnO reduce the initial bacterial load as well, but their antibacterial activity does not show significant differences against samples containing ZnO ($p \leq 0.05$). Finally, it must be noted that although such significant differences were detected, the maximal reduction does not go over one order of magnitude in comparison to the negative control. It can be observed that such reduction is around 1000 times for PCL:ZnO 6%, which is equivalent to a decrease of 96% of bacterial load in comparison to the negative control. A similar behavior is observed at samples with HA and ZnO, among these PCL:HA:ZnO 1% reduces almost 99% of the initial bacterial load. Finally, it must be noticed that after 0 and 30 days of degradation, on samples containing HA and ZnO, higher amounts of ZnO induce a decrease of antibacterial activity in comparison to samples with only ZnO, contrary to the findings reported by other authors [39,40]. Such behavior suggests that polymer degradation after 30 days may counter ZnO antibacterial effect.

3.6 Degradation assays: Morphology analysis

SEM micrographs obtained with secondary electrons of the scaffolds after 0, 5 and 15 days of degradations are shown in figure 6. As it can be seen, degradation clearly induces morphology changes. Compared against PCL samples, which maintain their structural integrity after 15 days under degradation, samples with ZnO and HA clearly show considerable structural modifications for the same period of time. Many cracks and notches can be seen at PCL:HA, PCL:ZnO and PCL:HA:ZnO after 15 days degradation. In particular, notches are mainly observed at samples with ZnO.

Degraded samples were dried, freeze-dried and subsequently weighed. After 15 days under degradation, the mass loss does not exceed 1% respect to initial mass (data not shown). Therefore, considering observed notches as well as the negligible mass loss and based on Vieira *et al.* observations, our results suggest that our scaffolds might be in an early stage of catalyzed erosion[41].

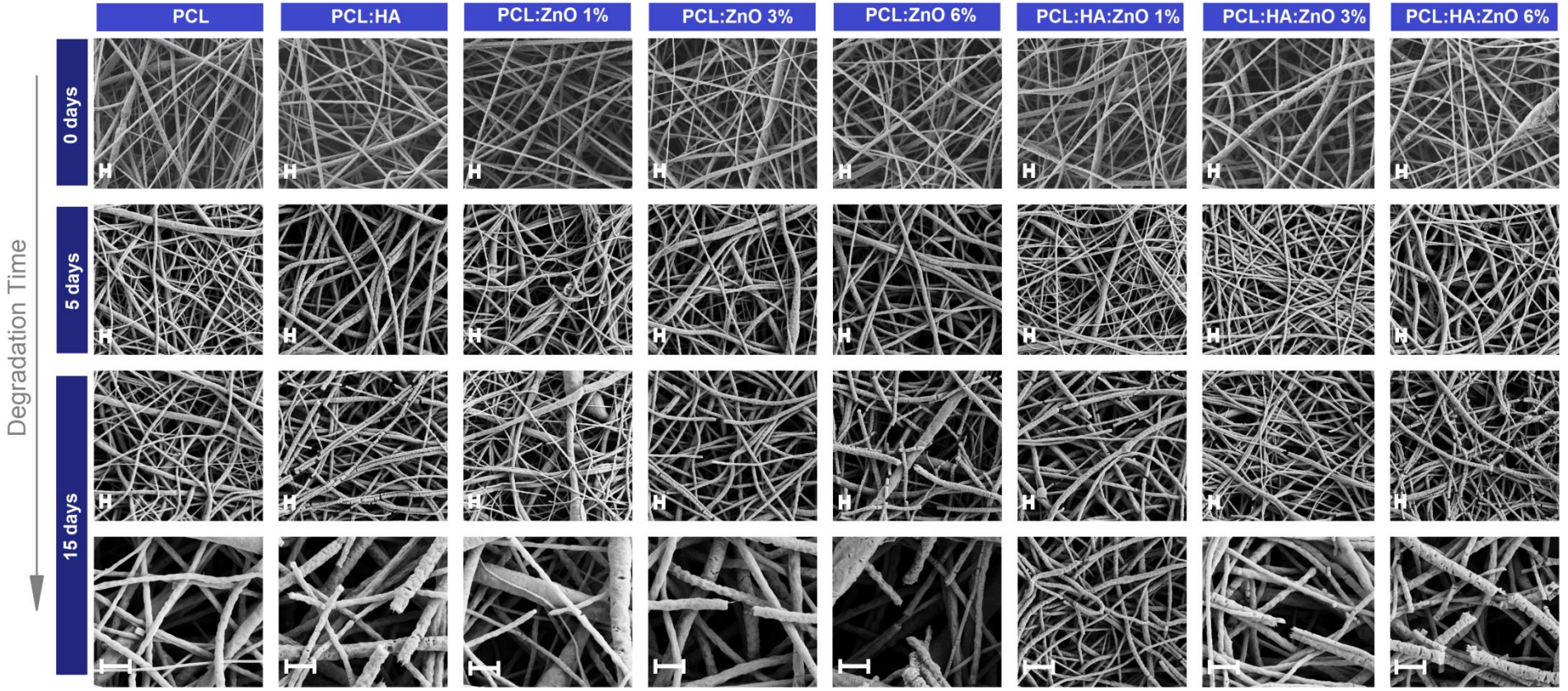

Figure 6 **SEM of scaffolds with different degradation times.** Micrographs of scaffolds with different ZnO content. PCL, PCL:HA, PCL:ZnO 1%, PCL:ZnO 3%, PCL:ZnO 6%, PCL:HA:ZnO 1%, PCL:HA:ZnO 3% and PCL:HA:ZnO 6%. Last row shows a zoom of samples after 15 days of degradation. Magnification bars are equal to 2 μm.

3.7 Mechanical properties

The assessment of mechanical properties of scaffolds before and after degradation is necessary to understand the degradation effects and also to elucidate the degradation mechanisms. Figure 7a presents typical stress-strain curves for PCL, PCL:HA, PCL:ZnO 3% and PCL:HA:ZnO 3% for 0, 5 and 15 days degradation. Figures 7b, 7c and 7d additionally show Young modulus, ultimate tensile strength and strain at fracture respectively for all samples.

Analysis of mechanical properties at day 0 indicates that both ZnO as well as HA particles reinforce the scaffolds. Particularly, the ultimate tensile strength plot suggests that maximal reinforcement is given by PCL:ZnO 3% and PCL:HA:ZnO 3%. Further increase of ZnO content up to 6% contrarily exerts an opposite effect on material resistance. This might be due to the reagglomeration of ZnO nanoparticles, as it was observed at SEM micrographs with backscattered electrons, and its resulting loss of interaction with polymeric matrix [31].

It can also be inferred from the bar plot shown in figure 7 that a marked decrease of mechanical properties is the main consequence of degradation advance. In particular, PCL:ZnO 3% and PCL:HA:ZnO 3% induce the greatest reduction of Young modulus (39% and 45% respectively), ultimate tensile strength (71% and 70%) and strain at fracture (76% and 84%) when compared against values at day 0 of degradation. In order to understand such response, the derivative of the ultimate tensile strength in function of time was obtained and analyzed. Such curves are shown in figure 8.

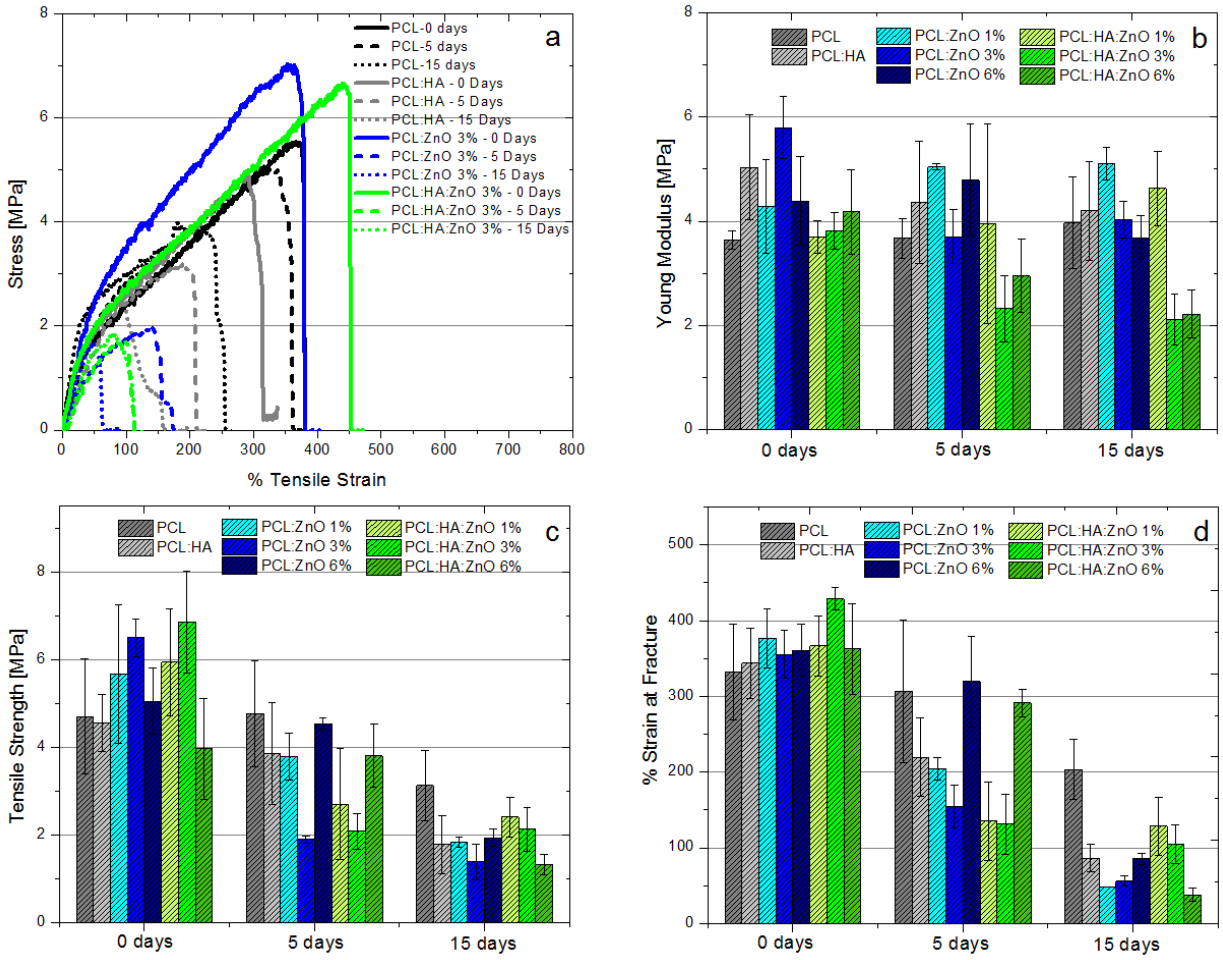

Figure 7 **Mechanical properties vs Degradation time.** (a) Stress-strain curves of PCL, PCL:HA, PCL:ZnO 3% y PCL:HA:ZnO 3% (b) Young modulus (c) Ultimate tensile strength (d) Strain at fracture.

First, these curves indicate that an increase of ZnO content up to 3% induces a significant increase of mechanical-resistance-loss rate. Second, curves show that the addition of HA particles also accelerates degradation. And third, curve shapes of PCL:ZnO 1 and 3% suggest that degradation of such samples is presumably the result of the combination of more than one degradation mechanism. These points will be further discussed in sections below.

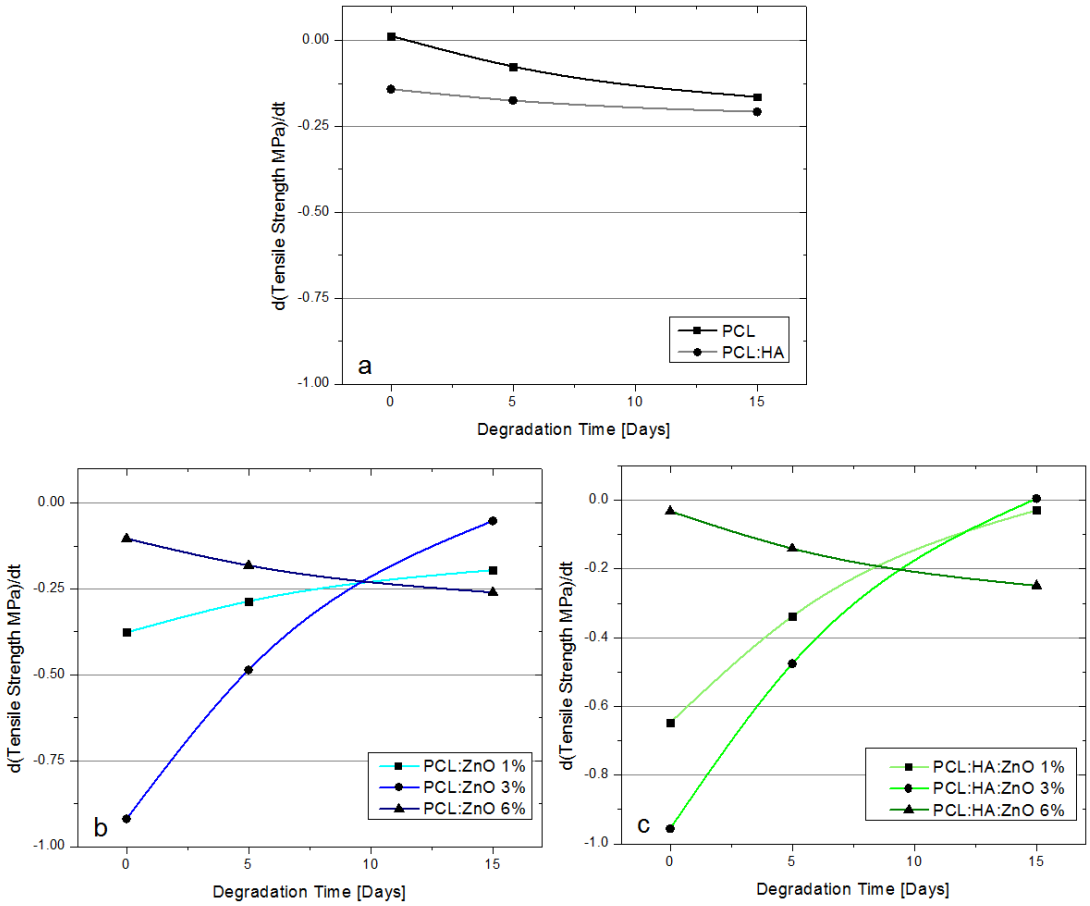

Figure 8 **Mechanical-resistance-loss rate.** Derivative of ultimate tensile strength in function of degradation time for (a) PCL and PCL:HA (b) PCL:ZnO 1, 3 and 6% (c) PCL:HA:ZnO 1, 3 and 6%.

3.8 Wettability

Surface hydrophobicity in function of ZnO and HA content was evaluated in terms of contact angle between sample surfaces and distilled water. As it can be seen in figure 9, ZnO and HA addition does not significantly decrease samples wettability (Welch Test, $p \leq 0.05$). Regardless of the slight contact angle decrease observed after ZnO and HA addition, such difference represents not more than 5% reduction against PCL contact angle. This suggests that most

particles might not be exposed on material surface so that they do not considerably affect intrinsic hydrophobicity of PCL.

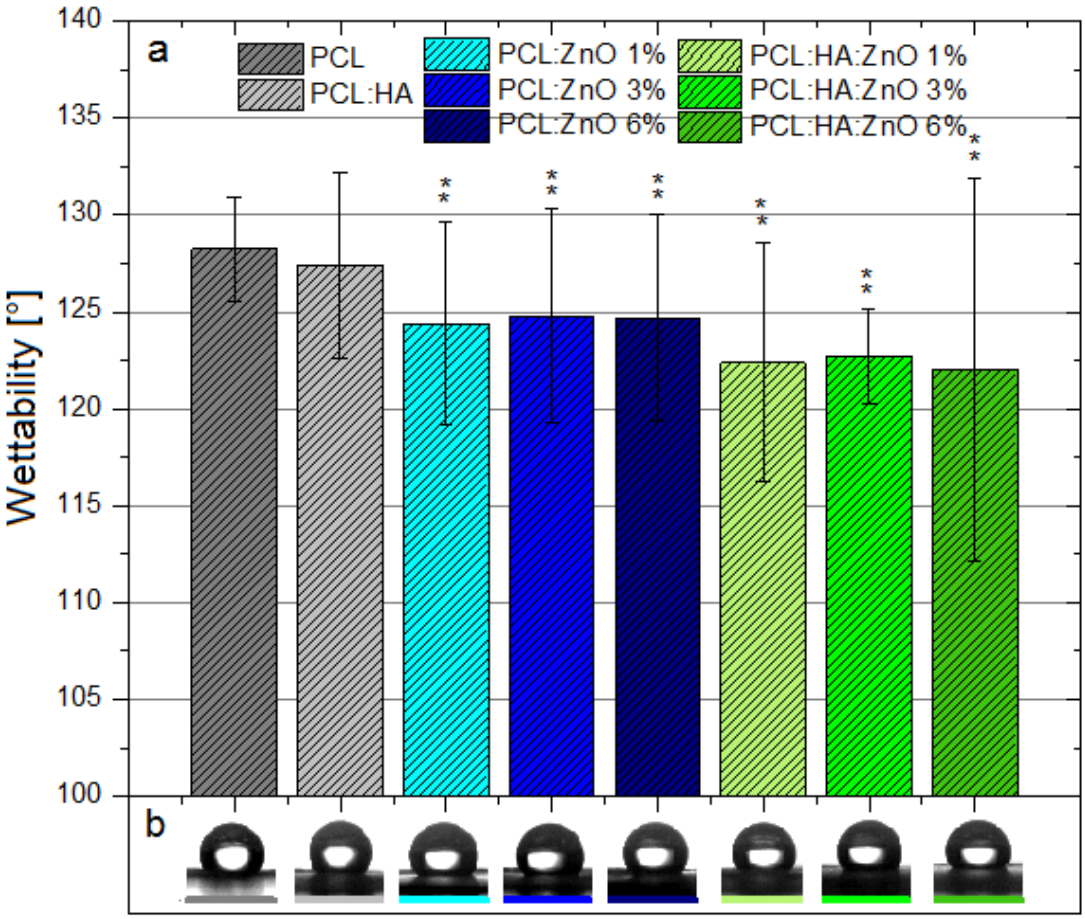

Figure 9 **Wettability vs % ZnO.** Contact angles between distilled water and sanples after 0 days of degradation. ** Statistical significance against PCL ($p \leq 0.5$).

Contact angles at samples subjected to 5 and 15 days of degradation were also assessed. Such samples were dried and subsequently freeze-dried. In all cases, contact angle was equal to 0° (data not shown), which proves a significant increase of sample wettability caused by material degradation. Contact angle depends on chemical composition as well as solid-liquid interaction. The presence of surface polar groups induces a decrease of contact angle due to a higher interaction between the surface and the polar solvent, water [42]. Then, our results

indicate that scaffold degradation might induce exposure of polar groups which noticeably increase scaffolds wettability.

3.9 Differential thermal analysis

A first approach for crystallinity study of our scaffolds was accomplished through DTA. Such analysis was used in order to determine the influence of ZnO and HA as well as degradation effect on Tm, which represents an indirect measure of polymer cristallinity[43]. Such values were obtained from the first scanning during sample heating. Theoretically, through DTA is also possible to assess Tc behavior in function of aforementioned parameters. However, given technical features at room temperature of the available DTA equipment and considering that Tc of PCL is comparable to room temperature, it was not feasible to accurately register Tc given the shift introduced by the measurement system at that temperature range [42,44].

Figure 10 presents endothermal melting peaks of the scaffolds after 0 and 15 days of degradation as a function of ZnO and HA content. As it can be seen, curves at 0 days suggest that ZnO addition induces a decrease of Tm respect to Tm of pure PCL samples. Additionally, these curves also show that such decrease is greater when ZnO is combined with HA. Whereas for PCL:ZnO samples Tm reduction is approximately 2°C, for PCL:HA:ZnO samples such decrease is around 3°C. In both cases, such shift suggests that ZnO particles might hinder nucleation and subsequent growth of lamellaes, which leads to thinner lamellae and therefore Tm shifting according to other studies [31,42,45]. It is worth noting that the Tm shifts among scaffolds with different ZnO contents are similar. This might be due to a weak interaction between the polymer matrix and our fillers[31]. Furthermore, it is remarkable that whereas samples with ZnO induce Tm shifts, such effect is not registered with non-degraded PCL:HA samples. Presumably, given the large HA particle size in comparison to ZnO

nanoparticles -and therefore, low surface-volume ratio such particles might not considerably hinder matrix crystallization [31].

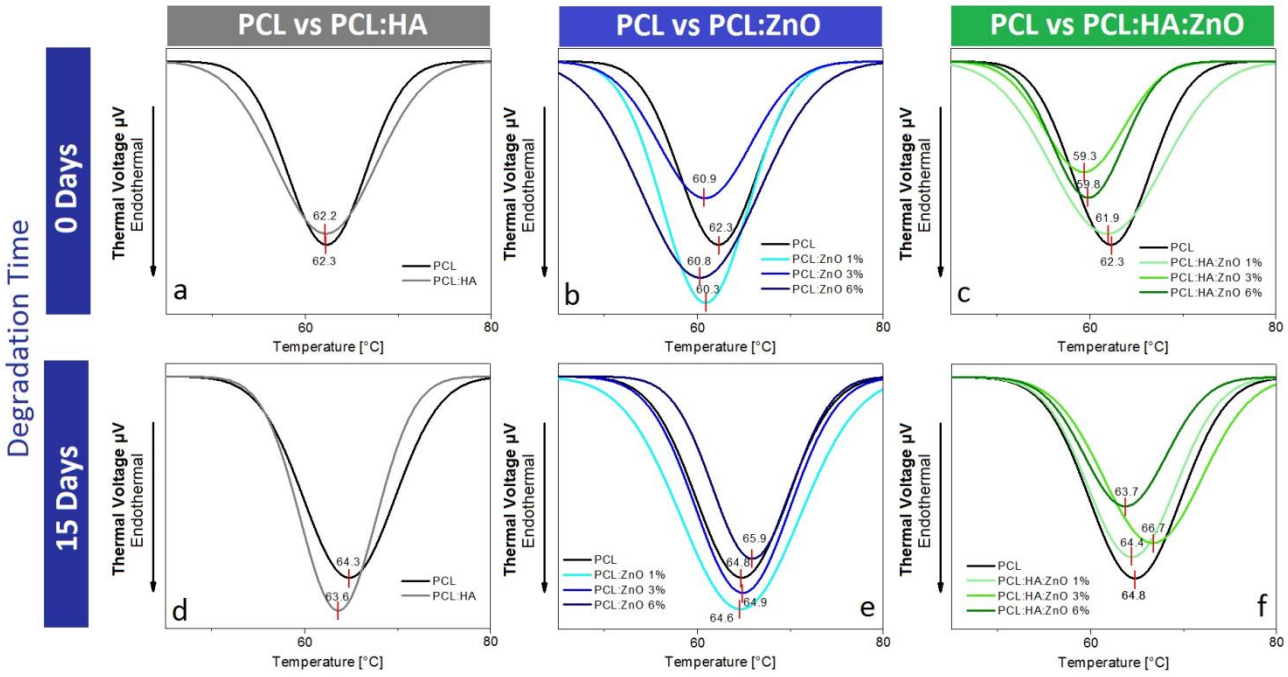

Figure 10 **Differential thermal analysis.** Melting temperature for samples (a,b,c) after 0 days of degradations and (d,e,f) after 15 days of degradation.

Samples degradation, as it can be also observed in figure 10, results in Tm increase in all cases. As Eldsäter *et al.* reported, amorphous phase of PCL is degraded before crystalline phase degradation [44,46]. The most accepted theory claims that this effect is caused by rapid diffusion of water into amorphous regions, resulting in a relative increase of material crystallinity which is reflected in an increase of Tm -as our graphs show [42,46,47]. Finally, it must be noted that after degradation, significant differences between Tm of samples with ZnO and Tm of pure PCL samples practically disappear. Such phenomenon was also reported by Eldsäter *et al.* during abiotic degradation of PCL [46].

3.10 Infrared spectroscopy

The hydrolytic degradation of our scaffolds was also assessed through FTIR. Figures 11 and 12 present FTIR spectra for all samples at 0, 5 and 15 days under degradation between 4000-1500 cm^{-1} and 1500-400 cm^{-1} respectively. Between 4000 and 1500 cm^{-1}, degradation induces a lower intensity of bands at 2942 cm^{-1} and 2863 cm^{-1} in comparison to the same bands at non-degraded samples. Such bands are related to C-H bond in saturated carbon atoms, and therefore, decrease of band intensity implies chain scission and its resulting loss of saturated carbons [42,48–50]. Furthermore, it must be noted a wide band of low intensity between 1500 and 1726 cm^{-1} in some degraded samples. Such band is related to C=O bond stretching at carboxyl groups and it is a consequence of PCL hydrolysis, which comprises an increase of terminal -COOH groups. This effect is also observed through an intensity increase at 1186-1116 cm^{-1} bands, which is associated to C-O bonds at carboxyl groups[48]. Moreover, the peak observed at 1726 cm^{-1} corresponds to ester bonds stretching at the main polymer chain (-CO) [42,48]. It is worth mentioning that whereas HA presence is clearly observed through bands at 569 cm^{-1} and 603 cm^{-1}, caused by flexion of bonds at phosphate groups, ZnO signals are not registered given their low intensity.

Finally, it must be pointed out that unlike other authors, new bands due to degradation are not observable e.g. at 3402 cm^{-1}. This band is related to OH stretching of carboxyl group and is typically observed at hydrolyzed PCL [42]. Such lack of bands was also observed by Peña *et al.* in PCL samples also degraded by immersion in PBS [49].

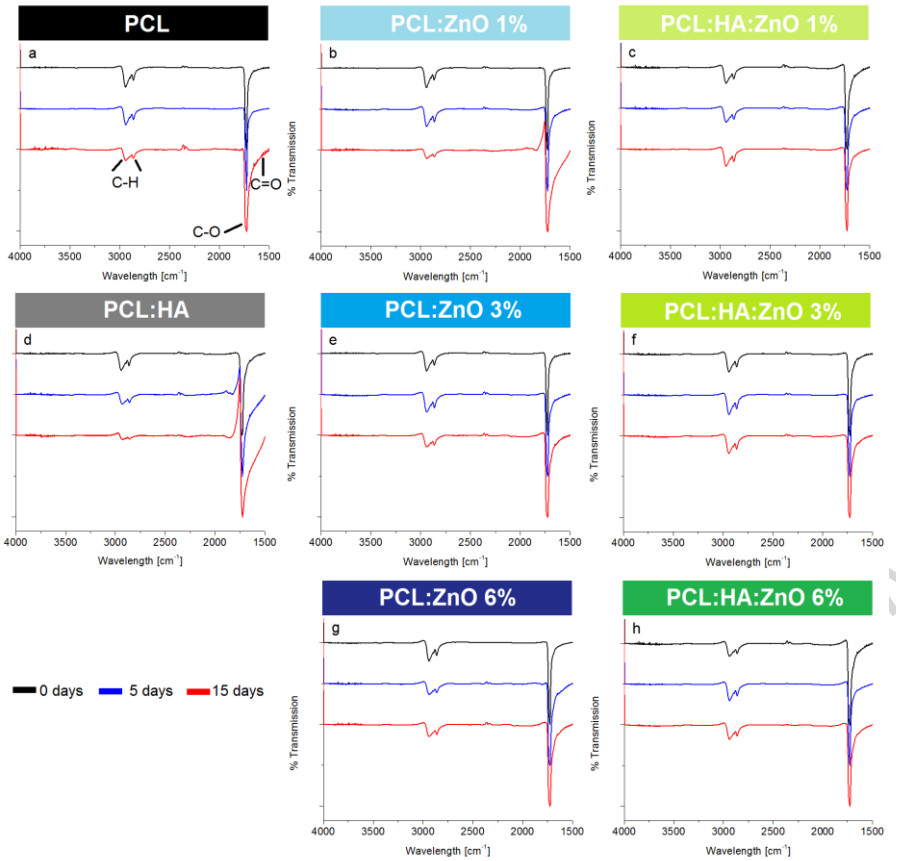

Figure 11 FTIR spectrum 4000-1500 cm^{-1} for (a) PCL (d) PCL:HA (b,e,g) PCL:ZnO 1, 3 and 6% y (c, f, h) PCL:HA:ZnO 1, 3 and 6% at 0, 5 and 15 days under degrdation.

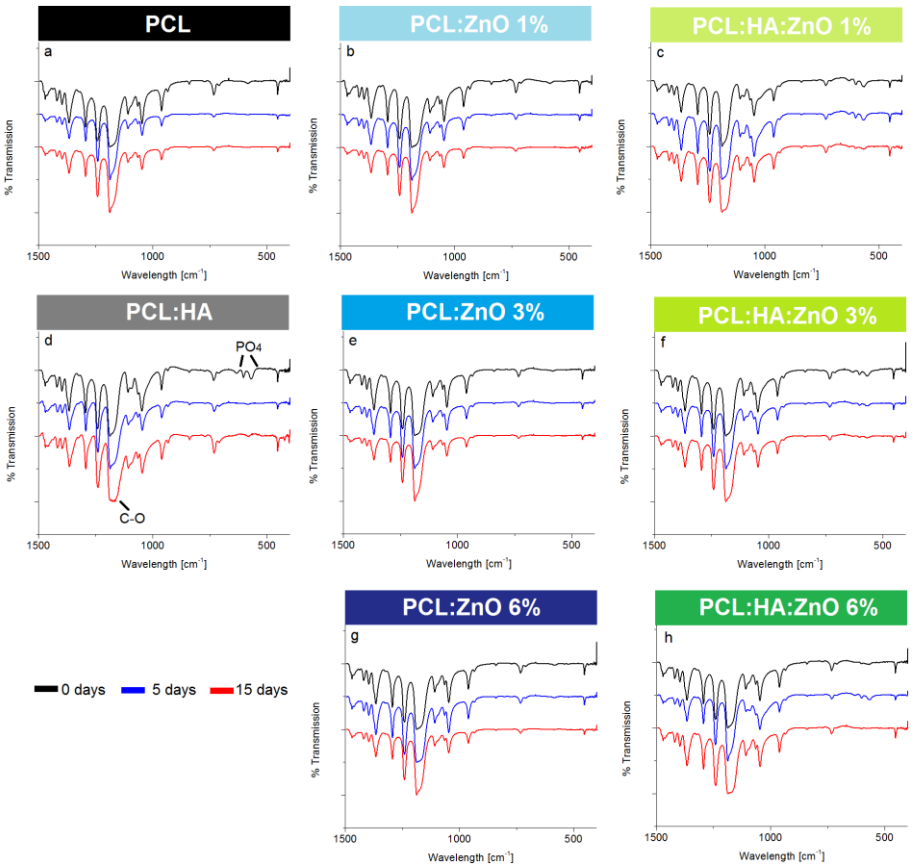

Figure 12 FTIR spectrum 1500-400 cm^{-1} for (a) PCL (d) PCL:HA (b,e,g) PCL:ZnO 1, 3 and 6% y (c, f, h) PCL:HA:ZnO 1, 3 and 6% at 0, 5 and 15 days under degradation. Degradation here is observed through band 1186-1116cm^{-1} (C-O).

4. DISCUSSION

Among the several challenges imposed by BTE, the acceleration of bone tissue regeneration is so far an issue. PCL has been widely used in BTE given its low toxicity, its degradability through hydrolysis and its long-term mechanical stability [10]. However, this polymer lacks of specific cues for bone regeneration and therefore modifications are necessary in order to optimize bone growth on PCL [9]. As a first modification, in this work PCL was processed through electrospinning, a technique able to produce nanofibrous structures which mimic extracellular matrix of immature bone [11,12]. As it was shown in Figure 1, resulting membranes were composed by random fibers with diameters ranging from 400 to 500 nm. Moreover, PCL was here combined and electrospun with HA and ZnO, both osteoconductive materials which due to their brittleness, may not be used by themselves as scaffolds. In this study, scaffolds were assessed in function of the ZnO content. *In vitro* cultures of HFOb in contact with electrospun mats were subjected to cell proliferation assays, ALP activity and ARS staining. Furthermore, antibacterial efficacy against *S. aureus* as well as *in vitro* degradation of our scaffolds in function of ZnO content were also here analyzed.

Cell proliferation analysis in combination with ALP activity and mineralization results suggested not only that higher concentrations of ZnO induced higher mineralization but also demonstrated that ZnO may act as a triggering molecule for mineralization of the scaffolds. Furthermore, the results presented in this study also indicated that ZnO and HA might have opposite effects, as it will be further discussed.

The main action mechanism of ZnO involves release of Zn^{2+} ions, as suggested by several previous studies [51–53]. Zn^{2+} seems to exert an anabolic effect on osteoblastic cells at intra and extracellular level. Intracellularly, Zn^{2+} ions primarily regulates Runx2 expression, a transcription factor directly related to osteoblastic differentiation and bone maturation[18,53–55]. In particular, Kwun *et al* demonstrated that Zn^{2+} deficiency delays the expression of Runx2 and consequently, mineralization of extracellular bone matrix [56]. Besides, at

extracellular level, the Zn^{2+} ion - a natural ALP co-factor - regulates the enzyme activity. The ALP is a dimer with very similar subunits. Each subunit (~69.000 Da) contains: (1) a Zn atom strongly bonded to a specific site, which contributes to structural integrity of the polypeptide; and (2) a Zn atom slightly bonded to the active site (Dean 2002). Thus, an increase of extracellular zinc induces an increase of ALP activity as Dean *et al*, Nagata *et al* and other authors already reported [57–61]. Therefore, the early triggering of mineralization inferred from the assays presented in this study as well as the increased amount of calcium deposits observed while increasing ZnO concentrations may be due to intracellular and extracellular effects of Zn^{2+}, respectively.

Mineralization triggering involves three stages. At the beginning, there is an active cell proliferation which is almost simultaneously followed by extracellular matrix maturation during a second stage. Once cell proliferation rate decreases, ALP activity increases, reaching thus a maximum of expression which consequently induces an optimization of extracellular matrix for subsequent mineralization, the third stage [36,62]. Owen *et al* further demonstrated that there is a reciprocal and functional relation between down-regulation of cell proliferation and osteoblastic differentiation [62]. Moreover, it must be considered that: (1) HA is minimally osteoinductive given its low solubility, in comparison to other calcium phosphates [14]; (2) HA exerts primarily an osteoconductive effect by increasing adhesion, migration and cell proliferation as well as promoting extracellular matrix maturation through increased expression of extracellular proteins like collagen and osteocalcin [63–66]; and (3) Zn^{2+}primarily induces early mineralization, as it was already mentioned. Then, based on aforementioned facts, it may be inferred that simultaneous use of HA and ZnO involve the opposite effects. Such consequence was evidenced by the low cell proliferation measured at samples with both ZnO and HA. Furthermore, such result in addition to a clear higher mineralization observed on PCL:ZnO 6% indicates prevalence of Zn^{2+} effect over HA, which induces relatively earlier mineralization of small-cell populations.

Regarding the microbiological assessment, the antibacterial activity of the scaffolds against *S. aureus* was evaluated by a modified dilution method based on CLSI standards. The results showed that scaffolds with ZnO both at 0 and 30 days of degradation have antibacterial activity against *S. aureus*. It was also shown the larger the ZnO content, the higher the antibacterial activity. In addition, the results suggest that the primary antibacterial action mechanism may be through release of Zn^{2+} ion, which seems to increase after 30 days of degradation.

Up to date, three antibacterial action mechanisms of ZnO have been frequently reported: (1) cell membrane disruption after contact with nano ZnO; (2) release of Zn^{2+} ions and (3) production of reactive oxygen species (ROS) through photocatalysis [19,67,68]. The latter mechanism was not evaluated in this study since the samples were incubated without UV irradiation, which is mandatory for ROS induction. Considering then that the strain *S. aureus* is 71% more sensitive to Zn^{2+} action that to ZnO contact, and that the dilution method primarily depends on dilution of an antibacterial agent, it can be inferred that the antibacterial activity determined may be due to release of Zn^{2+} ions [19]. In addition, as Pasquet *et al* showed, the amount of ions released is increased in samples with larger concentrations of ZnO, which clearly explains the increase of activity detected with higher contents of ZnO within the scaffolds [19].

Finally, considering the degradation assays here performed, our results suggested that ZnO dispersion within the fibers plays a fundamental role during material degradation. As it was noted in figure 8, these curves first indicated that an increase of ZnO content up to 3% induces a significant increase of mechanical-resistance-loss rate. Second, these curves showed that the addition of HA particles also accelerates degradation. And third, curve shapes of PCL:ZnO 1 and 3% suggested that degradation of such samples is presumably the result of the combination of more than one degradation mechanism. The first two points might be explained -partially, for samples with ZnO- in function of ZnO and HA particles themselves,

which act as stress concentrators. HA and ZnO particles might exert mechanical loads on polymer matrix leading then to hydrolysis acceleration, according to Díaz *et al.* and as it was observed by Augustine *et al.* at PCL scaffolds compounded with ZnO[28,42]. Regarding the third point, following facts must be considered: (1) Qu *et al.* demonstrated that ZnO acts as an external catalyst of polylactic acid (PLA) hydrolysis, an aliphatic polyester as PCL[69]; (2) Siparsky *et al.* proved that under autocatalysis or catalysis, degradation rate curve fits an exponential curve[70]; (3) given the low dissociation rate of terminal acid groups at PCL when compared against PLA, it is considered that autocatalysis at PCL practically does not occur[70]; (4) Vieira *et al.* showed that under non-catalyzed degradation conditions, ultimate tensile strength curves resembles the curves obtained during our assays[41]. Therefore, ultimate tensile strength curves and their derivatives suggest that both PCL:ZnO 1 and 3% as well as PCL:HA:ZnO 1 and 3% might be subjected to degradation as a result of combination of non-catalyzed hydrolysis of PCL and catalyzed *hydrolysis* around ZnO particles. Moreover, given mechanical loads applied by particles themselves, degradation is also accelerated. Strikingly, at PCL:ZnO and PCL:HA:ZnO 6% samples, ZnO-catalyzed *hydrolysis* component seems significantly decreased. Given the reduction of effective polymer-ZnO contact surface due to the high amount of large agglomerates at such scaffolds, the curves suggest that catalyzed-*hydrolysis* might be decreased.

5. CONCLUSIONS

This study demonstrated that PCL:ZnO scaffolds are suitable for bone tissue engineering. In particular, it was shown that such scaffolds, with relatively low concentrations of ZnO, may accelerate bone tissue regeneration by the increase of ALP activity followed by early mineralization. Moreover, opposite effects of HA and ZnO was also showed. It was further demonstrated that the scaffolds exert an antibacterial effect on *S. aureus*. Such activity increased with larger amounts of ZnO. Finally, our results clearly indicated that ZnO

nanopowder not only significantly accelerates samples degradation but also suggest that degradation rate might be regulated through variation of ZnO nanopowder concentration as well as through variation of ZnO dispersion within the fibers. Hence, it may be considered that the scaffolds here assessed are potentially suitable for BTE given their osteoactive features, its antibacterial skills and their ability to be degraded in short-, mid- and long-term depending on ZnO content and dispersion. Therefore, the scaffolds here studied might be competitive products against the clinical solutions nowadays applied in regenerative medicine

6. ACKNOWLEDGMENTS

Research conduction of this study was financed by the National Agency for Scientific and Technological Promotion (PDTS-CIN n°574, Argentina). Financial support from Ministry of Economy and Competitiveness (MINECO), Madrid (Grants BIO2013-41242-R and BIO2016-75751-R) and from Generalitat de Catalunya (2014SGR837) are also acknowledged. The authors would like to thank the members of the Centro Integral de Microscopía (CCT Tucumán, CONICET, Argentina) for their technical support during SEM. Dr. Mariana Pérez Ibarreche is gratefully acknowledged for her assistance during microbiological assays. The authors would like to especially thank Dr. Gastón Lagarrigue and Od. Gabriela Pacios (Laboratorio de Biomateriales, Facultad de Odontología, Universidad Nacional de Tucumán, Argentina) for kindly providing the equipment for mechanical testing. Finally, M.K.Cruz and M.I.Gómez would like to thank SCAIT for its financial support (Project 26D-517).

7. REFERENCES

[1] R. Dimitriou, E. Jones, D. McGonagle, P. V. Giannoudis, Bone regeneration: current concepts and future directions., BMC Med. 9 (2011) 1–10. doi:10.1186/1741-7015-9-66.

[2] A. Oryan, S. Alidadi, A. Moshiri, N. Maffulli, Bone regenerative medicine : classic options , novel strategies , and future directions, (2014) 1–27.

[3] J. Nishida, T. Shimamura, Methods of reconstruction for bone defect after tumor excision: a review of alternatives., Med. Sci. Monit. 14 (2008) RA107-13. doi:865803 [pii].

[4] J.R. Venugopal, Y. Zhang, S. Ramakrishna, In Vitro Culture of Human Dermal Fibroblasts on Electrospun Polycaprolactone Collagen Nano fibrous Membrane, Artif. Organs. 30 (2006) 440–446. doi:10.1111/j.1525-1594.2006.00239.x.

[5] H. Cao, K. Mchugh, S.Y. Chew, J.M. Anderson, The topographical effect of electrospun nanofibrous scaffolds on the in vivo and in vitro foreign body reaction, J. Biomed. Mater. Res. - Part A. 93 (2010) 1151–1159. doi:10.1002/jbm.a.32609.

[6] P. Fedorová, R. Srnec, J. Pěnčík, P. Schmid, E. Amler, L. Urbanová, A. Nečas, Mechanical testing of newly developed biomaterial designed for intra-articular reinforcement of partially ruptured cranial cruciate ligament: Ex vivo pig model, Acta Vet. Brno. 83 (2014) 55–60. doi:10.2754/avb201483010055.

[7] D.A. Zopf, C.L. Flanagan, M. Wheeler, S.J. Hollister, G.E. Green, Treatment of Severe Porcine Tracheomalacia With a 3-Dimensionally Printed, Bioresorbable, External Airway Splint, JAMA Otolaryngol. Neck Surg. 140 (2014) 66. doi:10.1001/jamaoto.2013.5644.

[8] K.-H. Schuckert, S. Jopp, S.-H. Teoh, Mandibular defect reconstruction using three-dimensional polycaprolactone scaffold in combination with platelet-rich plasma and recombinant human bone morphogenetic protein-2: de novo synthesis of bone in a single case., Tissue Eng. Part A. 15 (2009) 493–499. doi:10.1089/ten.tea.2008.0033.

[9] A. Abdal-Hay, K.C. In, J.K. Lim, Biocorrosion and osteoconductivity of PCL/nHAp composite porous film-based coating of magnesium alloy, Solid State Sci. 18 (2013) 131–140. doi:10.1016/j.solidstatesciences.2012.11.017.

[10] M.A. Woodruff, D.W. Hutmacher, The return of a forgotten polymer - Polycaprolactone in the 21st century, Prog. Polym. Sci. 35 (2010) 1217–1256. doi:10.1016/j.progpolymsci.2010.04.002.

[11] J. Lannutti, D. Reneker, T. Ma, D. Tomasko, D. Farson, Electrospinning for tissue engineering scaffolds, Mater. Sci. Eng. C. 27 (2007) 504–509. doi:10.1016/j.msec.2006.05.019.

[12] J.Y. Rho, L. Kuhn-Spearing, P. Zioupos, Mechanical properties and the hierarchical structure of bone, Med. Eng. Phys. 20 (1998) 92–102. doi:10.1016/S1350-4533(98)00007-1.

[13] J. Doshi, D.H. Reneker, Electrospinning process and applications of electrospun fibers, Conf. Rec. 1993 IEEE Ind. Appl. Conf. Twenty-Eighth IAS Annu. Meet. 35 (1993) 151–160. doi:10.1109/IAS.1993.299067.

[14] S. Samavedi, A.R. Whittington, A.S. Goldstein, Calcium phosphate ceramics in bone tissue engineering: A review of properties and their influence on cell behavior, Acta Biomater. 9 (2013) 8037–8045. doi:10.1016/j.actbio.2013.06.014.

[15] E. Nyberg, A. Rindone, A. Dorafshar, W.L. Grayson, Comparison of 3D-Printed Poly-ε-caprolactone Scaffolds Functionalized with Tricalcium Phosphate, Hydroxyapatite, Bio-Oss, or Decellularized Bone Matrix, Tissue Eng. Part A. (2016) ten.TEA.2016.0418. doi:10.1089/ten.TEA.2016.0418.

[16] W. Zhu, D. Guo, L. Peng, Y.F. Chen, J. Cui, J. Xiong, W. Lu, L. Duan, K. Chen, Y. Zeng, D. Wang, Repair of rabbit cartilage defect based on the fusion of rabbit bone marrow stromal cells and Nano-HA/PLLA composite material, Artif. Cells, Nanomedicine, Biotechnol. 45 (2017) 115–119. doi:10.3109/21691401.2016.1138482.

[17] X. Zhao, Y. Han, J. Li, B. Cai, H. Gao, W. Feng, S. Li, J. Liu, D. Li, BMP-2 immobilized PLGA/hydroxyapatite fibrous scaffold via polydopamine stimulates osteoblast growth, Mater. Sci. Eng. C. (2017). doi:10.1016/j.msec.2017.03.186.

[18] K. Yusa, O. Yamamoto, H. Takano, M. Fukuda, M. Iino, Zinc-modified titanium surface enhances osteoblast differentiation of dental pulp stem cells in vitro, Nat. Publ. Gr. (2016) 1–11. doi:10.1038/srep29462.

[19] J. Pasquet, Y. Chevalier, J. Pelletier, E. Couval, D. Bouvier, M.A. Bolzinger, The contribution of zinc ions to the antimicrobial activity of zinc oxide, Colloids Surfaces A Physicochem. Eng. Asp. 457 (2014) 263–274. doi:10.1016/j.colsurfa.2014.05.057.

[20] S. Sakka, Factors associated with early and late failure of dental implants., J. Investig. Clin. Dent. 3 (2012) 258–61. doi:10.1111/j.2041-1626.2012.00162.x.

[21] S. Sakka, P. Coulthard, Implant failure: Etiology and complications, Med. Oral Patol. Oral Cir. Bucal. 16 (2011) 42–44. doi:10.4317/medoral.16.e42.

[22] D. Schwartz-Arad, A. Laviv, L. Levin, Failure causes, timing, and cluster behavior: an 8-year study of dental implants., Implant Dent. 17 (2008) 200–207. doi:10.1097/ID.0b013e3181777906.

[23] C.-H. Lee, Y.S. Chung, S.H. Lee, H.-J. Yang, Y.-J. Son, Analyses of the factors influencing bone graft infection after delayed cranioplasty, J. Trauma Acute Care Surg. 73 (2012) 255–260. doi:10.1007/s00701-006-0740-6.

[24] F.C. Tenover, Mechanisms of Antimicrobial Resistance in Bacteria, Am. J. Med. 119 (2006). doi:10.1016/j.amjmed.2006.03.011.

[25] C. Sfeir, C. Ho, B.A. Doll, K. Azari, J.O. Hollinger, Fracture Repair, in: J.R. Lieberman, G.E. Friedlaender (Eds.), Bone Regen. Repair Biol. Clin. Appl., Humanna Press, 2005: pp. 21–43.

[26] J. Henkel, M.A. Woodruff, D.R. Epari, R. Steck, V. Glatt, I.C. Dickinson, P.F.M. Choong, M.A. Schuetz, D.W. Hutmacher, Bone Regeneration Based on Tissue Engineering Conceptions – A 21st Century Perspective J, Bone Res. 3 (2013) 216–248. doi:10.4248/BR201303002.

[27] M.A. Woodruff, D.W. Hutmacher, The return of a forgotten polymer - Polycaprolactone in the 21st century, Prog. Polym. Sci. 35 (2010) 1217–1256. doi:10.1016/j.progpolymsci.2010.04.002.

[28] E. Díaz, I. Sandonis, M.B. Valle, In vitro degradation of poly(caprolactone)/nHA composites, J. Nanomater. 2014 (2014). doi:10.1155/2014/802435.

[29] J. Kotek, D. Kubies, J. Baldrian, J. Kovářová, Biodegradable polyester nanocomposites: The effect of structure on mechanical and degradation behavior, Eur. Polym. J. 47 (2011) 2197–2207. doi:10.1016/j.eurpolymj.2011.09.005.

[30] H. Doyle, S. Lohfeld, P.E. McHugh, Evaluating the effect of increasing ceramic content on the mechanical properties , material microstructure and degradation of selective laser sintered PCL / b-TCP materials, Med. Eng. Phys. 37 (2015) 767–776.

[31] C. DeArmitt, M. Hancock, Filled Thermoplastics, in: R.N. Rothon (Ed.), Part. Polym. Compos., Rapra Technology Limited, United Kingdom, 2003: p. 397. doi:10.1016/0142-9418(96)00004-9.

[32] E. Díaz, I. Sandonis, I. Puerto, I. Ibañez, In Vitro Degradation of PLLA/nHA Composite Scaffolds, Polym. Eng. Sci. 54 (2013) 2571–2578. doi:10.1002/pen.23806.

[33] H.-J. Prins, a K. Braat, D. Gawlitta, W.J. a Dhert, D. a Egan, E. Tijssen-Slump, H. Yuan, P.J. Coffer, H. Rozemuller, A.C. Martens, In vitro induction of alkaline phosphatase levels predicts in vivo bone forming capacity of human bone marrow stromal cells., Stem Cell Res. 12 (2014) 428–40. doi:10.1016/j.scr.2013.12.001.

[34] BSI British Standards, BS EN ISO 10993-13:2009: Biological evaluation of medical devices - Part 13: Identification and quantification of degradation products from polymeric medical devices, 2009.

[35] Deutsches Institut für Normung e.V., DIN 55660-Teil 2: Bestimmung der freien Oberflächenenergie fester Oberflächen durch Messung des Kontaktwinkels, 2011.

[36] H. Orimo, The mechanism of mineralization and the role of alkaline phosphatase in health and disease., J. Nippon Med. Sch. 77 (2010) 4–12. doi:10.1272/jnms.77.4.

[37] N.S. Fedarko, P. Bianco, U. Vetter, P. Gehron Robey, Human Bone Cell Enzyme Expression and Cellular Heterogeneity : Correlation of Alkaline Phosphatase Enzyme Activity With Cell Cycle, J. Cell. Physiol. 114 (1990) 115–121.

[38] E.E. Golub, K. Boesze-Battaglia, The role of alkaline phosphatase in mineralization, Curr. Opin. Orthop. 18 (2007) 444–448. doi:10.1097/BCO.0b013e3282630851.

[39] R. Cai, H. Wang, M. Cao, L. Hao, L. Zhai, S. Jiang, X. Li, Synthesis and antimicrobial activity of mesoporous hydroxylapatite/zinc oxide nanofibers, Mater. Des. 87 (2015) 17–24. doi:10.1016/j.matdes.2015.08.004.

[40] N. Saha, K. Keskinbora, E. Suvaci, B. Basu, Sintering, microstructure, mechanical, and antimicrobial properties of HAp-ZnO biocomposites, J. Biomed. Mater. Res. - Part B Appl.

Biomater. 95 B (2010) 430–440. doi:10.1002/jbm.b.31734.

[41] A.C. Vieira, J.C. Vieira, J.M. Ferra, F.D. Magalhães, R.M. Guedes, A.T. Marques, Mechanical study of PLA-PCL fibers during in vitro degradation, J. Mech. Behav. Biomed. Mater. 4 (2011) 451–460. doi:10.1016/j.jmbbm.2010.12.006.

[42] R. Augustine, N. Kalarikkal, S. Thomas, Effect of zinc oxide nanoparticles on the *in vitro* degradation of electrospun polycaprolactone membranes in simulated body fluid, Int. J. Polym. Mater. Polym. Biomater. 65 (2016) 28–37. doi:10.1080/00914037.2015.1055628.

[43] T.R. Crompton, Degree of Crystallinity and Melting Temperature, in: Pract. Polym. Anal., Springer US, 1993: pp. 630–647.

[44] M.J. Jenkins, K.L. Harrison, The effect of crystalline morphology on the degradation of polycaprlactone in a solution of phospate buffer and lipase, Polym. Adv. Technol. 19 (2008) 1901–1906. doi:10.1002/pat.

[45] E.A. Münchow, M.T.P. Albuquerque, B. Zero, K. Kamocki, E. Piva, R.L. Gregory, M.C. Bottino, Development and characterization of novel ZnO-loaded electrospun membranes for periodontal regeneration, Dent. Mater. 31 (2015) 1038–1051. doi:10.1016/j.dental.2015.06.004.

[46] C. Eldsäter, B. Erlandsson, R. Renstad, A.C. Albertsson, S. Karlsson, The biodegradation of amorphous and crystalline regions in film-blown poly(??-caprolactone), Polymer (Guildf). 41 (2000) 1297–1304. doi:10.1016/S0032-3861(99)00278-5.

[47] Y. Tokiwa, B.P. Calabia, C.U. Ugwu, S. Aiba, Biodegradability of plastics, Int. J. Mol. Sci. 10 (2009) 3722–3742. doi:10.3390/ijms10093722.

[48] A.R. Hernández, O.C. Contreras, J.C. Acevedo, L.G.N. Moreno, Poly(ε-caprolactone) Degradation Under Acidic and Alkaline Conditions, Am. J. Polym. Sci. 3 (2013) 70–75. doi:10.5923/j.ajps.20130304.02.

[49] J. Peña, T. Corrales, I. Izquierdo-Barba, M.C. Serrano, M.T. Portol??s, R. Pagani, M. Vallet-Reg??, Alkaline-treated poly(e-caprolactone) films: Degradation in the presence or absence of fibroblasts, J. Biomed. Mater. Res. - Part A. 76 (2006) 788–797. doi:10.1002/jbm.a.30547.

[50] X.J. Loh, The Effect of pH on the hydrolytic degradation of Poly(e-caprolactone)-block-Poly(thylene glycol) copolymers, J. Appl. Polym. Sci. 127 (2013) 2046–2056. doi:10.1002/app.37712.

[51] G.A. Fielding, W. Smoot, S. Bose, Effects of SiO2 , SrO, MgO and ZnO dopants in TCP on osteoblastic Runx2 expression, J. Biomed. Mater. Res. A. 102 (2014) 2417–2426. doi:10.1016/j.immuni.2010.12.017.Two-stage.

[52] K.S. Suh, Y.S. Lee, S.H. Seo, Y.S. Kim, E.M. Choi, Effect of zinc oxide nanoparticles on the function of MC3T3-E1 osteoblastic cells, Biol. Trace Elem. Res. 155 (2013) 287–294. doi:10.1007/s12011-013-9772-y.

[53] G. Fielding, S. Bose, SiO2 and ZnO dopants in three-dimensionally printed tricalcium

phosphate bone tissue engineering scaffolds enhance osteogenesis and angiogenesis in vivo, Acta Biomater. 9 (2013) 9137–9148. doi:10.1016/j.actbio.2013.07.009.

[54] M. Yamaguchi, M. Goto, S. Uchiyama, T. Nakagawa, Effect of zinc on gene expression in osteoblastic MC3T3-E1 cells: Enhancement of Runx2, OPG, and regucalcin mRNA expressions, Mol. Cell. Biochem. 312 (2008) 157–166. doi:10.1007/s11010-008-9731-7.

[55] M. Hie, N. Iitsuka, T. Otsuka, A. Nakanishi, I. Tsukamoto, Zinc deficiency decreases osteoblasts and osteoclasts associated with the reduced expression of Runx2 and RANK, Bone. 49 (2011) 1152–1159. doi:10.1016/j.bone.2011.08.019.

[56] I.S. Kwun, Y.E. Cho, R.A.R. Lomeda, H.I. Shin, J.Y. Choi, Y.H. Kang, J.H. Beattie, Zinc deficiency suppresses matrix mineralization and retards osteogenesis transiently with catch-up possibly through Runx 2 modulation, Bone. 46 (2010) 732–741. doi:10.1016/j.bone.2009.11.003.

[57] R.L. Dean, Kinetic studies with alkaline phosphatase in the presence and absence of inhibitors and divalent cations, Biochem. Mol. Biol. Educ. 30 (2002) 401–407. doi:10.1002/bmb.2002.494030060138.

[58] M. Nagata, B. Lönnerdal, Role of zinc in cellular zinc trafficking and mineralization in a murine osteoblast-like cell line, J. Nutr. Biochem. 22 (2011) 172–178. doi:10.1016/j.jnutbio.2010.01.003.

[59] Y.-E. Cho, R.-A.R. Lomeda, S.-H. Ryu, H.-Y. Sohn, H.-I. Shin, J.H. Beattie, I.-S. Kwun, Zinc deficiency negatively affects alkaline phosphatase and the concentration of Ca, Mg and P in rats., Nutr. Res. Pract. 1 (2007) 113–119. doi:10.4162/nrp.2007.1.2.113.

[60] M. Yamaguchi, R. Yamaguchi, Action of zinc on bone metabolism in rats. Increases in alkaline phosphatase activity and DNA content., Biochem. Pharmacol. 35 (1986) 773–7. doi:10.1016/0006-2952(86)90245-5.

[61] A. Cerovic, I. Miletic, S. Sobajic, D. Blagojevic, M. Radusinovic, A. El-Sohemy, Effects of zinc on the mineralization of bone nodules from human osteoblast-like cells, Biol. Trace Elem. Res. 116 (2007) 61–71. doi:10.1007/s12011-007-9016-0.

[62] T.A. Owen, M. Aronow, V. Shalhoub, L.M. Barone, L. Wilming, M.S. Tassinari, M.B. Kennedy, S. Pockwinse, J.B. Lian, G.S. Stein, Progressive development of the rat osteoblast phenotype in vitro: Reciprocal relationships in expression of genes associated with osteoblast proliferation and differentiation during formation of the bone extracellular matrix, J. Cell. Physiol. 143 (1990) 420–430. doi:10.1002/jcp.1041430304.

[63] F. Yang, Wen-Jing-Dong, F.M. He, X.X. Wang, S.F. Zhao, G.L. Yang, Osteoblast response to porous titanium surfaces coated with zincsubstituted hydroxyapatite, Oral Surg. Oral Med. Oral Pathol. Oral Radiol. 113 (2012) 313–318. doi:10.1016/j.tripleo.2011.02.049.

[64] M. Ngiam, S. Liao, A.J. Patil, Z. Cheng, C.K. Chan, S. Ramakrishna, The fabrication of nano-hydroxyapatite on PLGA and PLGA/collagen nanofibrous composite scaffolds and their effects

in osteoblastic behavior for bone tissue engineering, Bone. 45 (2009) 4–16. doi:10.1016/j.bone.2009.03.674.

[65] H.W. Kim, E.J. Lee, H.E. Kim, V. Salih, J.C. Knowles, Effect of fluoridation of hydroxyapatite in hydroxyapatite-polycaprolactone composites on osteoblast activity, Biomaterials. 26 (2005) 4395–4404. doi:10.1016/j.biomaterials.2004.11.008.

[66] P.A. Ramires, A. Romito, F. Cosentino, E. Milella, The influence of titania/hydroxyapatite composite coatings on in vitro osteoblasts behaviour, Biomaterials. 22 (2001) 1467–1474. doi:10.1016/S0142-9612(00)00269-6.

[67] A. Sirelkhatim, S. Mahmud, A. Seeni, N.H.M. Kaus, L.C. Ann, S.K.M. Bakhori, H. Hasan, D. Mohamad, Review on zinc oxide nanoparticles: Antibacterial activity and toxicity mechanism, Nano-Micro Lett. 7 (2015) 219–242. doi:10.1007/s40820-015-0040-x.

[68] A. Joe, S.H. Park, K.D. Shim, D.J. Kim, K.H. Jhee, H.W. Lee, C.H. Heo, H.M. Kim, E.S. Jang, Antibacterial mechanism of ZnO nanoparticles under dark conditions, J. Ind. Eng. Chem. 45 (2017) 430–439. doi:10.1016/j.jiec.2016.10.013.

[69] M. Qu, H. Tu, M. Amarante, Y.Q. Song, S.S. Zhu, Zinc oxide nanoparticles catalyze rapid hydrolysis of poly(lactic acid) at low temperatures, J. Appl. Polym. Sci. 131 (2014) 1–7. doi:10.1002/app.40287.

[70] G.L. Siparsky, K.J. Voorhees, F. Miao, Hydrolysis of Polylactic Acid (PLA) and Polycaprolactone (PCL) in Aqueous Acetonitrile Solutions: Autocatalysis, J. Environ. Polym. Degrad. 6 (1998) 31–41. doi:10.1023/A:1022826528673.

VITAE

Betiana Felice. During the development of this work, Dr. Felice was a Doctoral Research Fellow at the National Council of Scientific and Technical Researches (CONICET, Argentina). She obtained her PhD and her degree in Biomedical Engineer from the National University of Tucumán (Argentina). Her research interests include biomaterials, nanotechnology, drug delivery systems and tissue engineering.

M. Alejandra Sánchez is currently a Post-Doctoral Research Fellow at the National Council of Scientific and Technical Researches (CONICET, Argentina). She obtained her degree as Biomedical Engineer from the National University of Tucumán (Argentina). Her research interests include antibacterial biomaterials, TiO_2 nanotubes and nanotechnology

M. Cecilia Socci is currently a Doctoral Research Fellow at the National Council of Scientific and Technical Researches (CONICET, Argentina). She obtained her degree as Biotechnologist from the National University of Tucumán (Argentina). Her research interests include electrospun scaffolds for regeneration of nervous tissue

Luciano D. Sappia is currently a Post-Doctoral Research Fellow at the National Council of Scientific and Technical Researches (CONICET, Argentina). Dr. Sappia obtained his PhD and his degree in Biomedical Engineering from the National University of Tucumán (Argentina). Currently his work is mainly focused on the development of biosensing platforms using conductive polymers.

María Inés Gómez is a professor of inorganic chemistry at the National University of Tucumán, where she also obtained her PhD. Dr. Gómez counts with multiple publications related to synthesis and analysis of inorganic components, her main research interest.

M. Karina Cruz is currently an experienced technician specialized in analysis techniques of inorganic and organic components like FTIR, DTA, DSC, etc. Mrs. Cruz has a degree in biochemistry, obtained at the National University of Tucumán.

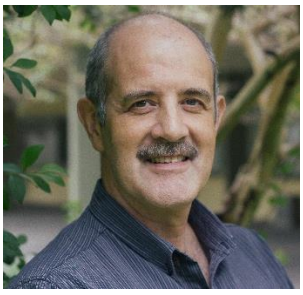

Carmelo J. Felice is a professor of biomedical transducers and impedancimetry at the National University of Tucumán and also head of the laboratory where this work was mostly performed. As main researcher of CONICET, Prof. Felice is advancing science and engineering aspects of biosensors, tissue engineering and neuroscience to realize their full potential in healthcare and environment. He is a highly cited scientist with his major focus nowadays on technology transference. He authored over 50 journal papers and 4 books in addition to 8 patents.

Mercè Martí is currently professor of immunology at the Autonomous University of Barcelona (Spain). Dr. Martí research is mainly focused on molecular biology of breast cancer cells as well as immunological alterations during AIDS and diabetes.

M. Isabel Pividori is tenured Professor at the Autonomous University of Barcelona (UAB, Spain). She leads a research team on bioanalytical chemistry and biosensing, particularly focused on the design of electrochemical biosensing devices and emerging technologies appropriate at community and primary-care level for clinical diagnosis and food safety in low resource settings. Prof. Pividori is a higly cited scientist, with an h-index of 34 and more than 3300 citations.

Gabriela Simonelli is professor of materials science at the National University of Tucumán. Dr. Simonelli is a researcher highly specialized on computational simulation of crystal lattices as well as synthesis and analysis of ZnO nanostructures intended for electrical applications. Dr. Simonelli obtained her PhD from the University of Buenos Aires and is an active member of multiple science societies.

Andrea P. Rodríguez is associate researcher at the National Council of Scientific and Technical Researches (CONICET, Argentina) and associate professor at the Bioengineering Department of the National University of Tucumán (Argentina). Prof. Rodríguez conducted her Ph.D. and Post-doctoral studies in the Department of Oral Pathology and Medicine, at the Okayama University (Japan). Her research interests have been mainly focused on bone tissue engineering, adipose tissue engineering, cell culture and cell-biomaterial interactions, with multiple publications in such fields.

Highlights

- We synthesized electrospun PCL scaffolds compounded with ZnO nanostructures and hydroxyapatite
- We evaluated the effect of the ZnO nanostructures and hydroxyapatite on the *in vitro* response of osteoblasts against our scaffolds as well as their antibacterial efficacy against *S. aureus*
- We evaluated the *in vitro* degradation of our scaffolds in function of ZnO content
- We demonstrated *in vitro* mineralization of our scaffolds as well as a significant antibacterial efficacy against *S. aureus*
- We demonstrated the acceleration and regulation of the degradation rate of our scaffolds by compounding with ZnO nanostructures.